

SCALING LAWS FOR MIXED QUANTIZATION

Zeyu Cao^{1*} Boyang Gu^{2*} Cheng Zhang² Pedro Gimenes² Jianqiao Lu³
 Jianyi Cheng⁴ Xitong Gao^{5,6} Yiren Zhao^{2†}

¹Department of Computer Science and Technology, University of Cambridge

²Department of Electrical & Electronic Engineering, Imperial College London

³Department of Computer Science, University of Hong Kong

⁴School of Informatics, University of Edinburgh

zeyu.cao@cl.cam.ac.uk, jqlu@cs.hku.hk, jianyi.cheng@ed.ac.uk

{boyang.gu19, cheng.zhang122, pedro.gimenes19, a.zhao}@ic.ac.uk

xt.gao@siat.ac.cn

ABSTRACT

Post-training quantization of Large Language Models (LLMs) has proven effective in reducing the memory and computational requirements for inference. In this study, we focus on a straightforward question: When aiming for a target accuracy or perplexity with low-precision quantization, how much high-precision computation needs to be preserved and how fine-grained this quantization would need to be as we scale LLMs to larger sizes? We first introduce two critical metrics named the quantization ratio (Q_r) and quantization block size (Q_b). The former measures the number of parameters quantized to low-precision arithmetic normalized by the total parameter count, whereas the latter defines the number of values within a block that share a scaling factor, akin to the block size concept introduced in the FP4 format in NVIDIA’s Blackwell architecture. Through extensive and carefully controlled experiments across different model and quantization methods, we propose a unified scaling law on post-training quantization (PTQ) that can predict loss degeneration for varying Q_r and Q_b . For Q_r , our scaling law implies that parameter scaling and ratio scaling have a multiplicative relationship. Consequently, larger models are more amenable to a higher quantization ratio Q_r , thus supporting an increase in the adoption of mixed quantization for inference. Regarding Q_b , our findings indicate that a small block size, similar to that used in Blackwell, is not essential for large models. Employing a small Q_b can instead unnecessarily complicate the design of the hardware circuit.

1 INTRODUCTION

Large language models (LLMs) have demonstrated remarkable performance in a range of natural language processing (NLP) tasks (Brown et al., 2020), and state-of-the-art models now contain billions of parameters (Anthropic, 2025; OpenAI, 2025; DeepMind, 2025). As such, researchers have attempted to understand the scaling laws of LLMs by characterizing how the required number of training tokens scales with parameter count to train compute-optimal models under a fixed compute budget (Kaplan et al., 2020; Hoffmann et al., 2022). These works provide insight into how to best allocate resources in training increasingly large LLMs.

Despite these training scaling laws, the substantial size of LLMs and their computational demands require significant hardware resources. As such, quantization has become a promising solution to increase the compute and memory efficiency of LLM inference (Lin et al., 2024; Chee et al., 2024; Ashkboos et al., 2024). The recently proposed Scaling Laws for Precision by Kumar et al. further examined the interplay among precision levels, model parameters, and data – they suggested a revised version of the Chinchilla form (Kaplan et al., 2020), with an additional error term to capture the impacts of post-training quantization (PTQ).

*Equal Contribution.

†Corresponding author.

Meanwhile, there is also an active research thread, which has shown that weights and activations in pre-trained transformer blocks often yield magnitude outliers (Gu et al., 2024). This issue has been tackled by assigning higher precision to outliers while putting the remainder of the network at lower precision (Dettmers et al., 2022; Zhang et al., 2023a; Dettmers et al., 2023). With the introduction of more compact arithmetic types in NVIDIA’s Blackwell GPUs, including the support for 4-bit and 6-bit MXFP formats (Tirumala & Wong, 2024). These arithmetic types, such as MX arithmetics, incorporate a block size Q_b , in which a set of values shares the same scaling factor. The first iteration of this concept, known as block floating point, dates back to the 1990s and was used in digital signal processing (Kobayashi & Fettweis, 1999). This can be seen as a granularity of quantization where, at $Q_b = 1$, the arithmetic resembles the traditional floating-point number format, comprising both a mantissa and an exponent for scaling purposes. Subsequently, this concept of blockwise scaling factors was adopted in the domain of low bitwidth quantization for neural networks (Dai et al., 2021; Lingle, 2023; Darvish Rouhani et al., 2020), including the recently available MX-format on the Blackwell GPUs. These hardware advancements enable both high- and low-precision computations on silicon, making **mixed-precision inference** a compelling approach to maintain model performance while reducing compute and memory costs.

Driven by the significance of developing systematic scaling laws to direct future research in mixed quantization, we aim to address a largely under-explored question: How does the optimal ratio of low-precision elements and the optimal granularity in a mixed quantization mapping change as the model size enlarges? Put another way, *what are the scaling laws that govern mixed quantization?*

For a pair of low- and high-precision parameters (W_l, W_h) , we define the mixed-quantization ratio Q_r as the ratio of parameters using low-precision arithmetic to the total number of parameters, and consider the scenario where this allocation happens normally only at the post-training stage. We consider block size granularities as Q_b for the block-based quantization methods. Then our search space over the respective random variable of low-precision and high-precision parameters $(\mathcal{W}_l, \mathcal{W}_h)$ for a given pair of Q_r and Q_b is as follows.

$$(\mathcal{W}_l, \mathcal{W}_h) \sim \left\{ (W_l, W_h) : \frac{\|W_l\|_0}{\|W_h\|_0 + \|W_l\|_0} = Q_r \wedge \mathcal{Q}_b(W_l, W_h) = Q_b \right\}, \quad (1)$$

where $\|\cdot\|_0$ refers to the l_0 norm, and $\mathcal{Q}_b(W_l, W_h)$ is the function that calculates the block size used for the searched quantization. We experimented with 3 different LLM model families and 4 different post-training quantization methods, covering weight-only and weight-activation (W-A) quantizations. In total, we applied mixed quantization to 17 models, with model sizes ranging from 60M to 14B, resulting in a total of 54,600 quantized model checkpoints.

For a language model with N parameters, trained on D tokens with a fixed quantization ratio Q_r and fixed block size Q_b , the loss can be considered a discrete random variable \mathcal{L} . The variation in loss is due to the combinatorial space among all possible combinations of low- and high-precision parameter pairs for the given Q_r and Q_b . Note that in our post-training quantization space, D is fixed for the given model. We describe a unified scaling law that formulates the model inference loss as the sum of the usual Chinchilla form with a post-training quantization loss degeneration term (Δ), which itself is also a discrete random variable defined similarly on $(\mathcal{W}_l, \mathcal{W}_h)$.

$$\mathcal{L}(N, D, Q_r, Q_b) = \underbrace{\underbrace{aN^{-\alpha}}_{\text{Training-time Effects}} + bD^{-\beta} + E}_{\text{Usual Chinchilla form}} + \underbrace{\Delta(N, Q_b, Q_r)}_{\text{Loss Degeneration}}, \quad (2)$$

where a, b, α, β , and E are constants.

We claim that the optimal (minimum) and expectation of Δ are the overall effect of ratio, parameter, and granularity scaling effects. *I.e.*,

$$\delta^{\text{opt}}(N, Q_r, Q_b) = \min(\Delta(N, Q_r, Q_b)) = C \cdot \underbrace{e^{AQ_r}}_{\text{ratio scaling}} \cdot \underbrace{N^{-\gamma_N}}_{\text{parameter scaling}} \cdot \underbrace{(Q_b + d)^{\gamma_c}}_{\text{granularity scaling}}, \quad (3)$$

$$\mathbb{E}[\delta(N, Q_r, Q_b)] = C' e^{A'Q_r} N^{-\gamma'_N} (Q_b + d')^{\gamma'_c}, \quad (4)$$

respectively, where $A, A', C, C', \gamma_N, \gamma'_N, d, d', \gamma_c$, and γ'_c are constant coefficients. This finding also suggests a strong link to the prior work conducted by Kumar et al.. If $Q_r = 1$ and Q_b are fixed as constants, Equation (3) agrees asymptotically with the Precision Scaling Law proposed by Kumar et al. (Section 2). We make the following contributions:

1. **Unified Scaling Law on PTQ with ratio and granularity scaling.** We propose a unified scaling law that considers both the mixed quantization ratio Q_r and quantization block size granularity Q_b , and its expectation and minimum forms reach asymptotic agreement with existing Precision Scaling Laws shown by Kumar et al.. Our scaling laws integrate model sizes, mixed quantization ratios, and quantization granularities, thereby extending the scope beyond existing scaling laws that focus solely on precision levels.
2. **Ratio matters more.** Our scaling law indicates that, since $\mathcal{O}(e^{AQ_r})$ grows faster than $\mathcal{O}(N^{\gamma_N})$, the growth of Q_r dominates the quantization loss. However, although e^{AQ_r} growth faster than N^{γ_N} asymptotically, Q_r can only be 1 at most while N can grow without a limit, showing that larger models can accommodate a progressively larger quantization ratio. This effectively shows that mixed quantization is a promising future direction for further reducing model sizes and model computation complexity.
3. **The quantization ‘‘strength’’ provides diminishing returns at large model sizes.** Since γ_c is within 0 and 1 with our scaling law (See Section 2), lowering Q_r is more effective than lowering Q_b related terms, allowing better quantization performance.

2 SCALING LAWS FOR MIXED QUANTIZATION

Our scaling law can be considered a further development of the previous Precision Scaling Law (Kumar et al., 2024). The usual Chinchilla form (Hoffmann et al., 2022) suggests that for a language model with a total number of parameters N , trained on a number of tokens D , its loss L should scale as follows.

$$L(N, D) = aN^{-\alpha} + bD^{-\beta} + E, \quad (5)$$

where a, b, α, β and E are positive constants. The Precision Scaling Law (Kumar et al., 2024) further investigates the case where post-training quantization is applied. In detail, following previous notations, if the model is trained and tested (inferred) at different precisions P_{train} and P_{post} , Equation (5) becomes

$$L(N, D, P_{\text{train}}, P_{\text{post}}) = aN_{\text{eff}}^{-\alpha} + bD^{-\beta} + E + \delta_{\text{PTQ}}(N_{\text{eff}}, D, P_{\text{train}}, P_{\text{post}}), \quad (6)$$

where δ is the post-training quantization loss degeneration. It has the following form:

$$\delta_{\text{PTQ}}(N, D, P_{\text{train}}, P_{\text{post}}) = C_T e^{-P_{\text{post}}/\gamma_{\text{post}}} \left(\frac{D^{\gamma_D}}{N^{\gamma_N}} \right) \prod_{x \in \{w, a, kv\}} [1 - e^{-C_x(P_x - P_{\text{post}})}], \quad (7)$$

where P_w, P_a, P_{kv} are the weight, activation, and kv-cache precision bit-width at training, and $C_T, \gamma_{\text{post}}, \gamma_D, \gamma_N$, and C_x -s are constants. Such a scaling law for the loss degeneration was developed under the consideration that the quantization setting is applied to all weights. Equation (7), proposed by Kumar et al. (2024), only allows the degree of freedom to quantize the combination of weight, activation, and KV-cache. However, different quantization configurations should also be considered for mixed quantization inference. To investigate this aspect, we introduce the quantization ratio Q_r and the quantization block size Q_b .

Consider a model M with size N , with a block size Q_b , we define the block number as $N_b = N/Q_b$. As $M = \{m_i\}_{i=1}^N$, we define a partition of M into N_b blocks, i.e. $\mathcal{B} = \{b_j = m_{(j-1) \cdot Q_b + 1 : j \cdot Q_b}\}_{j=1}^{N_b}$. Given a codebook collection $\mathcal{C} = \{C_k\}_{k=1}^{N_c}$ of size N_c where each codebook C_k is a binary partition function over \mathcal{B} to a pair of low- and high-precision components, i.e., $C_k(b_i) = (W_l^{(i,k)}, W_h^{(i,k)})$, we further define a mapping $f : \mathcal{B} \rightarrow \{j\}_{j=1}^{N_c}$ according to the quantization setting. Then we denote $\mathcal{Q}_b(W_l, W_h) = Q_b$ as saying that the block size is Q_b for

$$(W_l, W_h) = \left(\bigcup_{j=1}^{N_b} C_{f(b_j)}^0(b_j), \bigcup_{j=1}^{N_b} C_{f(b_j)}^1(b_j) \right). \quad (8)$$

For a given quantization ratio (Q_r) and quantization block size (Q_b), there are different pairs of (W_l, W_h) . The set of all possible pairs forms the binary discrete random variable (W_l, W_h) . For each pair of (W_l, W_h) , we could calculate the corresponding quantized model loss and post-quantization loss degeneration, with a bit of abuse of notation, Equation (6) turns into its random variable form

$$\mathcal{L}(N, D, Q_r, Q_b) = aN^{-\alpha} + bD^{-\beta} + E + \Delta(N, Q_b, Q_r), \quad (9)$$

where \mathcal{L} and Δ are the random variable forms of L and δ respectively.

We define the optimal allocation of low-precision parameters for a model under Q_r and Q_b as $(W_l^{\text{opt}}, W_h^{\text{opt}})$, where it minimizes the loss L . *I.e.*,

$$(W_l^{\text{opt}}, W_h^{\text{opt}}) = \arg \min_{(W_l, W_h)} L(W_l, W_h) \quad \text{s.t.} \quad \frac{\|W_l\|_0}{\|W_h\|_0 + \|W_l\|_0} = Q_r \wedge \mathcal{Q}_b(W_l, W_h) = Q_b. \quad (10)$$

It is easily seen that the pair $(W_l^{\text{opt}}, W_h^{\text{opt}})$ minimizes the loss degeneration δ too. Equation (10) outlines the optimization problem used to evaluate the hypothesized scaling laws. Note that the number of candidate pairs (W_l, W_h) explodes with the weight numbers. In this work, we find an approximate solution to the problem using a random search algorithm to allocate a numerical precision to each network component (*i.e.*, layer or matrix multiply operation, according to the quantization method). We estimate the expectation via its unbiased estimator. For n observed loss degeneration $(\delta_i)_{i=1}^n$, $\mathbb{E}(\delta)$ is approximated by

$$\mu_\delta((\delta_i)_{i=1}^n) = \frac{\sum_{i=1}^n \delta_i}{n}. \quad (11)$$

With a larger number of random search trials, we get a more precise estimate of loss degeneration. However, we discovered that even a small amount of random sampling of Δ could reveal its distribution quite successfully. Detailed discussion of this phenomenon can be seen in Appendix B.

Recall Equation (9), since $(W_l^{\text{opt}}, W_h^{\text{opt}})$ is obtained from a group of candidates, we rewrite Equation (9) to the form of its best realization

$$L^{\text{opt}}(N, D, Q_r, Q_b) = aN^{-\alpha} + bD^{-\beta} + E + \delta^{\text{opt}}(N, Q_r, Q_b), \quad (12)$$

$$\delta^{\text{opt}}(N, Q_r, Q_b) = \delta(W_l^{\text{opt}}, W_h^{\text{opt}}). \quad (13)$$

Similarly, one may be interested in the expectation loss degeneration $\mathbb{E}(\Delta)$ rather than the optimal value. The expectation counterpart of Equation (12) is

$$\mathbb{E}[\mathcal{L}(N, D, Q_r, Q_b)] = aN^{-\alpha} + bD^{-\beta} + E + \mathbb{E}[\Delta(N, Q_r, Q_b)]. \quad (14)$$

Instead of studying the scaling law of one model, we focus on the **minimum loss a group of models can achieve optimally**. Furthermore, no weight training is performed after quantization to observe immediate performance degradation. We claim that such optimality also follows its own scaling. We describe the observed scaling laws and present empirical evidence to support them in Section 3.

Parameter scaling in Equation (2) Given a fixed Q_r , the optimal and expected loss degeneration $(\delta^{\text{opt}}, \mathbb{E}(\Delta))$ decreases polynomially as the model size $N = \|W_h^{\text{opt}}\|_0 + \|W_l^{\text{opt}}\|_0$ increases.

Ratio scaling in Equation (2) Given a fixed model size (N), the optimal and expected loss degeneration $(\delta^{\text{opt}}, \mathbb{E}(\Delta))$ increases exponentially as the quantization ratio Q_r increases.

Those two scaling laws posit one of our central hypotheses: the loss degeneration is affected by both the model size and the quantization ratio. We further discovered that their effects are independent. Therefore, we claim the following weak law of loss degeneration:

Weak Law of Loss Degeneration. Given a fixed quantization block size Q_b , a fixed quantization method, a model architecture that can scale its parameters N and change the quantization ratio Q_r . Following previous definitions, the optimal (minimum) and expectation of the loss degeneration have the following form:

$$\delta^{\text{opt}}(N, Q_r) = C e^{A Q_r} N^{-\gamma_N}, \quad (15)$$

$$\mathbb{E}[\Delta(N, Q_r)] = C' e^{A' Q_r} N^{-\gamma'_N}, \quad (16)$$

where C, C', A, A', γ_N , and γ'_N are constant coefficients that vary with different quantization block sizes and methods.

We could interpret e^{AQ_r} and $N^{-\gamma_N}$ as the quantization scaling effect and parameter scaling effect, respectively. Note that our scaling law is an extension of the precision scaling law shown in Equation (7). For $Q_r = 1$, the only possible pair is $(W_l, W_h) = (\emptyset, M)$. In such a case, our random variable Δ degenerates into its only realization, and the quantization scaling effect is absorbed into the coefficient C . On the other hand, if we fix D , P_{train} , and P_{post} in Equation (7), it leaves us with only a term of model size N that aligns with our parameter scaling effect.

In the weak law of loss degeneration, while δ^{opt} increases with Q_r exponentially, a larger model size N could compensate for such degeneration. Quantitatively, by fixing the loss budget $\delta^{\text{opt}} = l$, we have the following:

$$\log(N) = A''Q_r + C'', \quad (17)$$

where $A'' = A/\gamma_N$ and $C'' = (\log(C) - \log(l))/\gamma_N$. This shows that given a fixed loss budget ($\delta = l$), the maximum achievable mixed precision quantization ratio Q_r increases as the model size N increases. This aligns with findings from related research, such as AWQ (Lin et al., 2024), Quip (Chee et al., 2024), and LQER (Zhang et al., 2024), which empirically demonstrated that larger models can accommodate more aggressive quantization levels. An alternative view, also reflected in related work, is that for a fixed quantization ratio, task loss decreases when the model size becomes larger.

The weak scaling law is sufficient for the case where only the model size (N) and the quantization ratio Q_r are taken into consideration. If we want to estimate the loss degeneration with respect to the quantization block size Q_b , a stronger scaling law is needed. In fact, the scaling effect of granularity (block size) is also independent from the model size N and quantization ratio Q_r .

Strong Law of Loss Degeneration. Given a fixed quantization method, a model architecture that can scale its parameters N , change the quantization ratio Q_r , and vary its quantization block size Q_b . Following previous definitions, the optimal (minimum) and expectation of the loss degeneration has the following form:

$$\delta^{\text{opt}}(N, Q_r, Q_b) = Ce^{AQ_r}N^{-\gamma_N}(Q_b + d)^{\gamma_c}, \quad (18)$$

$$\mathbb{E}[\Delta(N, Q_r, Q_b)] = C'e^{A'Q_r}N^{-\gamma'_N}(Q_b + d')^{\gamma'_c}, \quad (19)$$

where $A, A', C, C', \gamma_N, \gamma'_N, d, d', \gamma_c$, and γ'_c are constant coefficients that depend on the quantization method.

For the strong scaling law, when fixing the quantization block size Q_b , the granularity scaling effect $(Q_b + d)^{\gamma_c}$ can be absorbed into the constant C in the weak law, indicating the effectiveness of the weak law for the case where Q_b is fixed.

3 EXPERIMENTS

3.1 SETUP

Models and benchmarks We evaluate a range of model families, including LLaMA (Touvron et al. (2023); Dubey et al. (2024a)), Qwen-1.5 (Bai et al. (2023)) and Qwen-3 (Qwen Team (2025)), at sizes ranging from 60M to 14B. Besides these models, to collect the mixed quantization results at small-scale models for extrapolation, we followed the Chinchilla scaling law and pretrained a series of LLaMA-like models consisting of $N \in \{60M, 200M, 400M, 600M, 1.1B\}$ parameters on FineWeb (Lozhkov et al., 2024), a high-quality pretraining dataset released by HuggingFace. We refer to these models as CLM series models to differentiate them from the vanilla Meta LLaMA models. More details are available in Appendix A. We choose Qwen-1.5 and Qwen-3 to validate our experimental results, enabling detailed analysis of the proposed scaling laws. We subsample a set of 1000 entries from the SlimPajama (Soboleva et al. (2023)) dataset for evaluation, which is another open-sourced pretraining dataset, as the perplexity/pretraining loss on SlimPajama better captures the performance of these base models compared with downstream tasks (Dubey et al., 2024b).

Quantization methods We mainly use MXINT (Rouhani et al. (2023)), and HQQ (Badri & Shaji (2023)) at various bit-widths and block sizes for low-precision formats, and BF16 as the high-

precision format. Specifically, if not mentioned specifically, by default, all our experiments are performed under weight-and-activation quantization with MXINT-4. We also include weight-and-activation quantized MXINT-2, weight-only quantized MXINT-4, and weight-only HQQ with 4 bit-widths and 64 block sizes to verify that our scaling laws apply to other data formats. We choose HQQ because it is a calibration-free method that achieves state-of-the-art performance, simplifying our search loop.

Mixed quantization strategy For our primary experiments, we perform quantization at two granularities: layer-wise and matmul-wise. In the former, the quantization ratio is determined by the number of transformer layers cast to low precision. In the latter, we consider the precision for each individual matrix multiplication. We find a solution for Equation (3) by searching through random trials of 100 from each quantization configuration. We justify these choices in Appendix Appendix B. For clarity, our experiments include a quantization ratio $Q_r \in \{0.5, 0.6, 0.7, 0.8, 0.9, 0.95, 0.975\}$. Note that, in each trial, the inner loop of the search conducts post-training quantization (PTQ), and the entire search process involves no training.

Platform and GPU hours We perform experiments on a cluster of DGX A100 eight-GPU pods, each with 40GB VRAM, with roughly 15k A100 GPU hours in total. We also spend around 1k GPU hours tuning search hyper-parameters, such as determining the number of trials and searching the loss landscape to determine an appropriate quantization ratio. The pretraining of CLM models takes around 1k GPU hours on another DGX H100 eight-GPU pod.

3.2 INSIGHTS FROM THE UNIFIED SCALING LAW

We mainly show results of the layer-wise loss landscape to verify our claims, but the same laws can also be applied to matrix multiplication-wise (matmul-wise). We present CLM, Llama, and QWen-3 in the main texts. All additional results, *e.g.*, matmul-wise and QWen-1.5, are in Appendix D.

3.2.1 MODEL SIZE (N) AND QUANTIZATION RATIO (Q_r)

Figure 1 shows the actual and fitted δ^{opt} for layer-wise MXINT-4 quantization for CLM series and Qwen3. The overall shape of the contour is the same for actual and fitted losses, with the statistics of $R^2 = 0.98$. As introduced in Section 2, the loss degeneration scaling law also works for the expectation value $\mathbb{E}(\delta)$, with a $R^2 = 0.99$, indicating the effectiveness of our law for $\mathbb{E}(\Delta)$. The corresponding figures and fitted parameters can be seen in Appendix F. From the results in Figure 1, we can make the following observations that are in line with our weak law:

Observation 1: With an increasing N , we can further increase Q_r , which is in agreement with our combined ratio scaling and parameter scaling terms: $e^{AQ_r} N^{-\gamma_N}$.

3.2.2 QUANTIZATION RATIO (Q_r) AND QUANTIZATION BLOCK SIZE (Q_b)

As stated in Section 4, recent LLM quantization methods adopt fine-grained quantization, meaning tensors are split into small blocks, quantized and then scaled individually. In this part, we empirically verify our unified scaling law by performing mixed-precision quantization search at blocksize $Q_b \in \{16, 32, 64, 128, 256\}$. We present the experiments on CLM series models with matrix-multiplication-wise for finer granularities. As shown in Figure 2, the overall shape of the contour is the same for actual and fitted losses on δ^{opt} , with the statistics $R^2 = 0.95$. From Section 2, the loss degeneration scaling law also works for the expectation value $\mathbb{E}(\delta)$, with a $R^2 = 0.98$, indicating the effectiveness of our law for $\mathbb{E}(\Delta)$. The corresponding figures and fitted parameters are in Appendix F. From the results in Figure 1, we can make the following observations that are in line with our strong law:

Observation 2: When the quantization ratio Q_r is low, employing a smaller block size Q_b is more effective in minimizing performance degradation, which agrees with our combined ratio scaling and granularity scaling terms: $e^{AQ_r}(Q_b + d)^{\gamma_c}$.

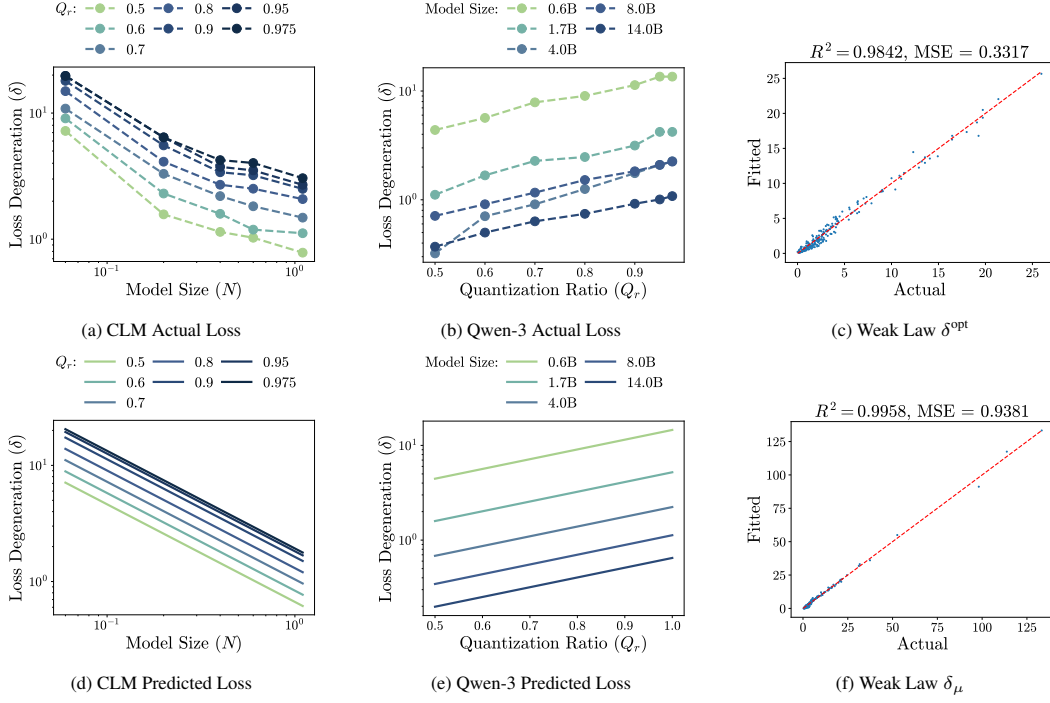


Figure 1: **Weak law experiment results.** (a,b,d,e): The actual and fitted loss degeneration contour for the layer-wise MXINT4 quantization for CLM and Qwen3 architecture. (a,d): Loss contour w.r.t. model size N for the CLM model family. (b,e): Loss contour w.r.t. quantization ratio Q_r for the Qwen3 model family. (e, f): The fitted versus actual δ^{opt} and δ_μ for all MXINT-4 quantization (layer- and matrix multiplication-wise) for CLM, Qwen1.5, and Qwen3. Due to space constraint, we only present N v.s. δ for CLM and Q_r v.s. δ in the figure, see Appendices C and D for full figures of all results.

3.3 EXTENDING TO OTHER QUANTIZATION METHODS

All our previous experiments consider W-A quantization with MXINT-4 as mentioned in Section 3.1. We also experimented with different quantization settings. For comparison, we showed that the loss degeneration scaling law still holds for other arithmetic formats and quantization methods. Moreover, as proposed by Dotzel et al. (2024), we consider weight-only quantization (with activations kept at 16-bit) for the precision allocation search. The results are presented in Figure 3. All three quantization settings follow our scaling law with different fitted parameters. Note that changing the precision (MXINT-4 and MXINT-2) will shift the parameters completely, which is different from the previous precision scaling law in Equation (7). Additional results are in Appendix E.

Observation 3: Our unified scaling law can be applied to other arithmetic formats.

3.4 LESSONS LEARNED

As discussed in Section 2, our weak scaling law aligns with the precision scaling law when $Q_r = 1$. Also, the strong scaling law that introduced the quasi-polynomial term did not deviate our scaling law away from the precision scaling law.

Takeaway 1: Across different Q_r values, our unified scaling law agrees asymptotically with previously proposed Precision Scaling Laws proposed by Kumar et al. (2024).

To observe the effect of different quantization ratios Q_r when varying model size N , we plot Figure 4a based on our unified scaling law on the CLM series model by fixing the δ budget. **When models are beyond 70B, Q_r can be set to beyond 0.9 with less than $\delta = 0.5$ loss degeneration.**

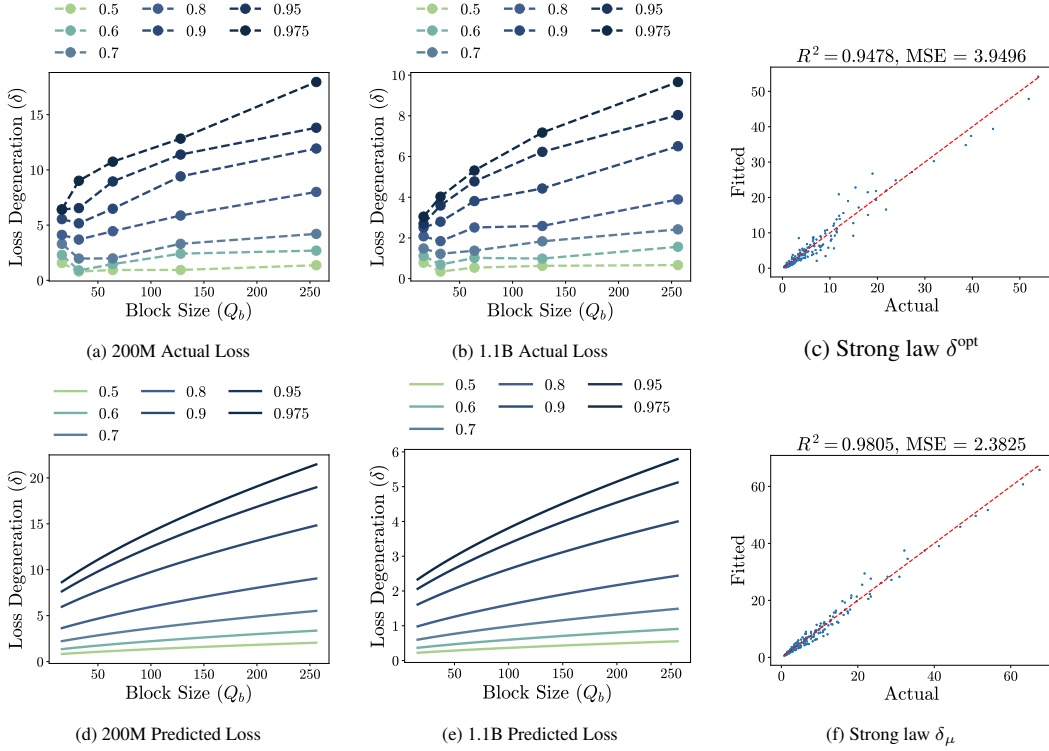


Figure 2: **Strong law experiment results.** (a,b,c,d): The actual and fitted loss degeneration contour for CLM-200M and CLM-1.1B w.r.t. block size Q_b . Each line corresponds to a fixed quantization ratio (Q_r). (e,f): The fitted versus actual δ^{opt} and δ_μ . Due to space constraint, we only present $N = 200M, 1.1B$, see Appendix C for full figures of all N blocksize results.

Takeaway 2: With an increase in model size, the quantization ratio Q_r can be set to a high value. This is due to the parameter scaling term in Equation (2) accelerating at a much faster rate compared to the ratio scaling.

For different block size granularities Q_b when varying model size N , we plot Figure 4b based on our unified scaling law on CLM series model. **This demonstrates that when the models are larger than 50B, the difference between $Q_b = 128$ and $Q_b = 32$ is less than 0.5 in terms of loss degeneration δ .** This makes us challenge the design choice of the current 128 block size utilized in NVIDIA’s Blackwell GPUs for Mixed-Precision Floating-Point (MXFP) arithmetic might be unnecessarily large for PTQ LLM inference tasks.

Takeaway 3: As the model size N becomes sufficiently large, changing the block size Q_b may yield diminished returns.

4 BACKGROUND AND RELATED WORK

Quantization outliers and mixed quantization A weight or activation value is considered an outlier when there is a significant deviation from its mean distribution. Activation outliers have been observed more frequently in large models (Wei et al., 2022; Zhang et al., 2023a) as cascaded layers accumulate quantization errors. In weight-only quantization, weights are mapped to low precision (Frantar et al., 2022; Lin et al., 2024). Recent weight-only quantization works focus on efficient vector quantization that maps high-precision weight tensors into indices and codebooks, such as QuiP (Chee et al., 2024), AQLM (Egiazarian et al., 2024), and QTIP Tseng et al. (2024). Meanwhile, weight-activation quantization usually transfers activation magnitudes to weights using invertible scale matrices (Xiao et al., 2023) before quantizing both weights and activations (Wei et al., 2023; Xiao et al., 2023; Shao et al., 2023). Recent works explore incoherence processing to

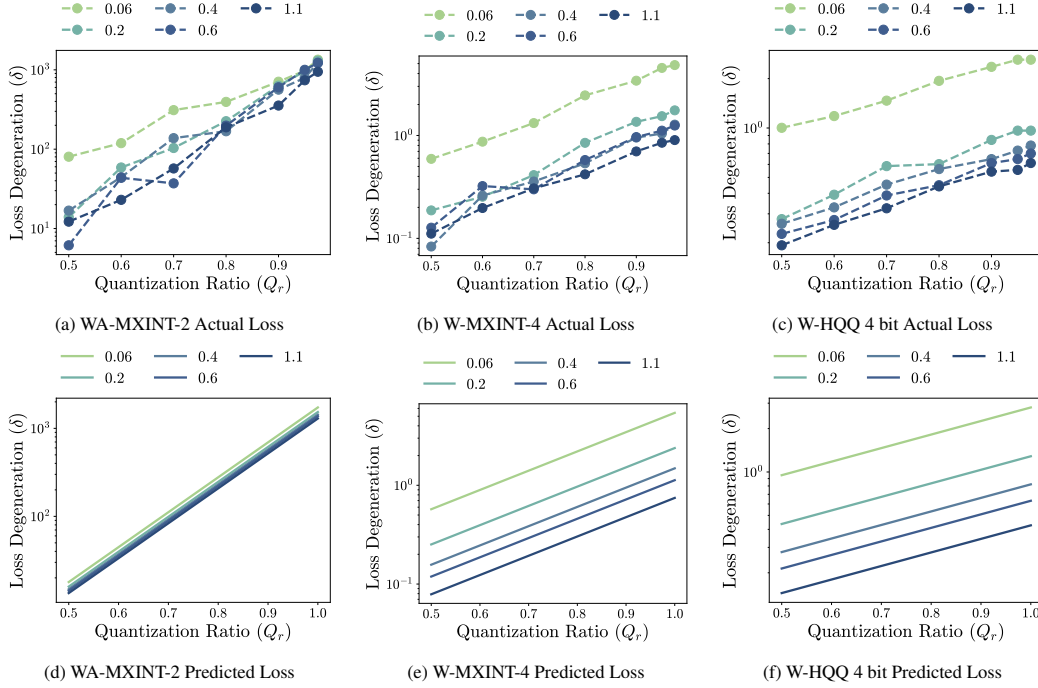


Figure 3: **Other Arithmetic Formats Results.** (a,d) The actual and fitted loss degeneration contour for layer-wise Weight-Activation-MXINT-2 (WA-MXINT-2) on CLM architectures. (b,e) The actual and fitted loss degeneration contour for layer-wise Weight-only MXINT-4 (W-MXINT-4) on CLM architectures. (c,f) The actual and fitted loss degeneration contour for layer-wise Weight-only Weight-only 4bit-HQQ (HQQ-4) on CLM architectures. In the figure, each line corresponds to a fixed model size N in billions (B). The fitted statistics are presented in Appendix F due to space constraint.

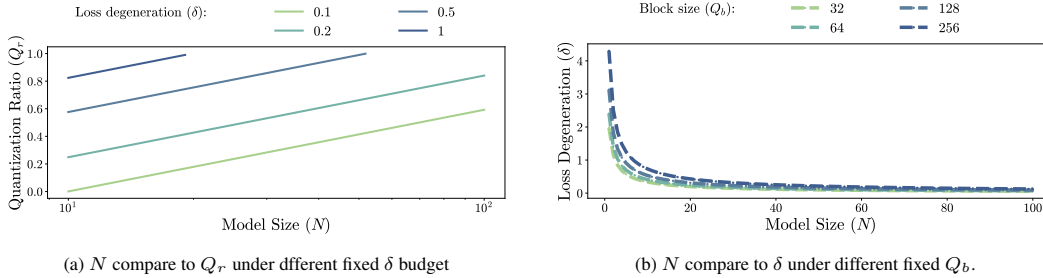


Figure 4: **Effects of our scaling laws.** The effect of our scaling law with (a) effect of quantization ratio Q_r when changing model size N under a fixed loss degeneration budget δ and (b) effect of blocksize granularities Q_b on loss degeneration δ when changing N . Both are based on the fitted parameters for CLM series models.

achieve this, such as SpinQuant (Liu et al., 2024b) and Quarot (Ashkboos et al., 2024). There are also works that solve the outlier problem via new number formats to accommodate the dynamic range of outliers (Zhang et al., 2023a; Rouhani et al., 2023; Zou et al., 2024). For example, MXINT/MXFP (Darvish Rouhani et al., 2020) is a recent standard for hardware-efficient numerical formats. MXINT shares an exponent across a block of mantissas (Rouhani et al., 2023), and MXFP shares an exponent across a block of MiniFloats, which is already supported in NVIDIA Blackwell. The hardware efficiency of these methods often outperforms standard low-precision floating-point computation, although custom hardware support is required.

Scaling laws of LLM training Kaplan et al. (2020) showed, through empirical analysis, that Transformer performance follows a power law trend. In contrast, Chinchilla Hoffmann et al. (2022) argues that existing LLMs are under-trained relative to their size, and parameter count should be

increased in line with the number of training tokens. The findings from [Pearce & Song \(2024\)](#) later explained the discrepancy between Kaplan and Hoffman, reaffirming the validity of the Chinchilla scaling laws. A highly relevant study is the recently proposed Scaling Laws for Precisions by [Kumar et al. \(2024\)](#). This work focuses on both pre-training and post-training quantization in which all parameters within the models are uniformly quantized to a single precision level. We discuss more in Section 2 into the relevance of our mixed quantization scaling laws, showing that in extreme cases, our unified mixed quantization law simplifies to adhere to the Scaling Laws for Precisions ([Kumar et al., 2024](#)).

5 DISCUSSION, LIMITATION AND CONCLUSION

Implications on AI inference hardware and systems We show that larger models can accommodate increasingly more low-precision components without performance degradation. This validates the recent trend of increasing support for low-precision arithmetic computation in hardware such as GPUs and TPUs [Tirumala & Wong \(2024\)](#); [Choquette \(2022\)](#). The insight from our unified scaling law highlights the **need for increased low-precision resources in future hardware devices**.

Extension to further architectures and arithmetic formats It is natural to consider whether the observed findings in this work extend to larger LLMs, such as 400B ones. Additionally, the same trends could be explored in more architectures including MoE models such as DeepSeek ([Liu et al., 2024a](#)) and Mixtral ([Jiang et al., 2024](#)). Finally, further arithmetic formats such as ternary ([Chen et al., 2024](#)) and additional configurations from the MXINT ([Rouhani et al., 2023](#)) standard offer opportunities for further exploration. One specific challenge is the quantization approach used in this paper is emulated following [Zhang et al. \(2023b\)](#), where it incurs more computation, hence impedes the evaluation of larger models (*e.g.*, 400B). A possible future direction would be to test these scaling laws on large models using actual MXINT4 and MXFP4 quantization upon the availability of compatible hardware.

Hypotheses on other efficient AI methods While we focused primarily on quantization, a clear direction for future research involves examining scaling trends for other Efficient AI methods, such as sparsity. We hypothesize that the scaling laws for such methods will closely resemble the scaling laws for quantization introduced in this work. More broadly, we hypothesize the existence of **a broader scaling law governing how the ratio of approximate compute to exact compute scales with model sizes**, and the granularity at which approximate compute is applied.

Conclusion In this paper, we introduce a unified scaling law for PTQ of LLMs, supported by thorough experiments. We explore the implications of this law on mixed quantization strategies and the selection of quantization block sizes. Our findings provide direction for future LLM quantization research and suggest a potential for mixed-quantization LLM inference accelerators.

REFERENCES

- Anthropic. Claude 3.7 sonnet system card. Technical report, Anthropic, February 2025.
- Saleh Ashkboos, Amirkeivan Mohtashami, Maximilian Croci, Bo Li, Pashmina Cameron, Martin Jaggi, Dan Alistarh, Torsten Hoefer, and James Hensman. Quarot: Outlier-free 4-bit inference in rotated llms. *Advances in Neural Information Processing Systems*, 37:100213–100240, 2024.
- Hicham Badri and Appu Shaji. Half-quadratic quantization of large machine learning models, November 2023. URL https://mobiusml.github.io/hqq_blog/.
- Jinze Bai, Shuai Bai, Yunfei Chu, Zeyu Cui, Kai Dang, Xiaodong Deng, Yang Fan, Wenbin Ge, Yu Han, Fei Huang, et al. Qwen technical report. *arXiv preprint arXiv:2309.16609*, 2023.
- Tom Brown, Benjamin Mann, Nick Ryder, Melanie Subbiah, Jared D Kaplan, Prafulla Dhariwal, Arvind Neelakantan, Pranav Shyam, Girish Sastry, Amanda Askell, et al. Language models are few-shot learners. *Advances in neural information processing systems*, 33:1877–1901, 2020.
- Jerry Chee, Yaohui Cai, Volodymyr Kuleshov, and Christopher M De Sa. Quip: 2-bit quantization of large language models with guarantees. *Advances in Neural Information Processing Systems*, 36, 2024.
- Tianqi Chen, Zhe Li, Weixiang Xu, Zeyu Zhu, Dong Li, Lu Tian, Emad Barsoum, Peisong Wang, and Jian Cheng. Ternaryllm: Ternarized large language model. *arXiv preprint arXiv:2406.07177*, 2024.
- Jack Choquette. Nvidia hopper gpu: Scaling performance. In *2022 IEEE Hot Chips 34 Symposium (HCS)*, pp. 1–46. IEEE Computer Society, 2022.
- Steve Dai, Rangha Venkatesan, Mark Ren, Brian Zimmer, William Dally, and Brucek Khailany. Vs-quant: Per-vector scaled quantization for accurate low-precision neural network inference. *Proceedings of Machine Learning and Systems*, 3:873–884, 2021.
- Bitva Darvish Rouhani, Daniel Lo, Ritchie Zhao, Ming Liu, Jeremy Fowers, Kalin Ovtcharov, Anna Vinogradsky, Sarah Massengill, Lita Yang, Ray Bittner, et al. Pushing the limits of narrow precision inferencing at cloud scale with microsoft floating point. *Advances in neural information processing systems*, 33:10271–10281, 2020.
- Google DeepMind. Gemini 2.5 pro preview, April 2025. Product page.
- Tim Dettmers, Mike Lewis, Younes Belkada, and Luke Zettlemoyer. Gpt3. int8 (): 8-bit matrix multiplication for transformers at scale. *Advances in Neural Information Processing Systems*, 35: 30318–30332, 2022.
- Tim Dettmers, Ruslan Svirschevski, Vage Egiazarian, Denis Kuznedelev, Elias Frantar, Saleh Ashkboos, Alexander Borzunov, Torsten Hoefer, and Dan Alistarh. Spqr: A sparse-quantized representation for near-lossless llm weight compression. *arXiv preprint arXiv:2306.03078*, 2023.
- Jordan Dotzel, Yuzong Chen, Bahaa Kotb, Sushma Prasad, Gang Wu, Sheng Li, Mohamed S Abdelfattah, and Zhiru Zhang. Learning from students: Applying t-distributions to explore accurate and efficient formats for llms. *arXiv preprint arXiv:2405.03103*, 2024.
- Abhimanyu Dubey, Abhinav Jauhri, Abhinav Pandey, Abhishek Kadian, Ahmad Al-Dahle, Aiesha Letman, Akhil Mathur, Alan Schelten, Amy Yang, Angela Fan, et al. The llama 3 herd of models. *arXiv preprint arXiv:2407.21783*, 2024a.
- Abhimanyu Dubey, Abhinav Jauhri, Abhinav Pandey, Abhishek Kadian, Ahmad Al-Dahle, Aiesha Letman, Akhil Mathur, Alan Schelten, Amy Yang, Angela Fan, et al. The llama 3 herd of models. *arXiv preprint arXiv:2407.21783*, 2024b.
- Vage Egiazarian, Andrei Panferov, Denis Kuznedelev, Elias Frantar, Artem Babenko, and Dan Alistarh. Extreme compression of large language models via additive quantization. *arXiv preprint arXiv:2401.06118*, 2024.

- Elias Frantar, Saleh Ashkboos, Torsten Hoefler, and Dan Alistarh. Gptq: Accurate post-training quantization for generative pre-trained transformers. *arXiv preprint arXiv:2210.17323*, 2022.
- Xiangming Gu, Tianyu Pang, Chao Du, Qian Liu, Fengzhuo Zhang, Cunxiao Du, Ye Wang, and Min Lin. When attention sink emerges in language models: An empirical view. *arXiv preprint arXiv:2410.10781*, 2024.
- Jordan Hoffmann, Sebastian Borgeaud, Arthur Mensch, Elena Buchatskaya, Trevor Cai, Eliza Rutherford, Diego de Las Casas, Lisa Anne Hendricks, Johannes Welbl, Aidan Clark, Tom Hennigan, Eric Noland, Katie Millican, George van den Driessche, Bogdan Damoc, Aurelia Guy, Simon Osindero, Karen Simonyan, Erich Elsen, Jack W. Rae, Oriol Vinyals, and Laurent Sifre. Training compute-optimal large language models, 2022. URL <https://arxiv.org/abs/2203.15556>.
- Wei Huang, Haotong Qin, Yangdong Liu, Yawei Li, Xianglong Liu, Luca Benini, Michele Magno, and Xiaojuan Qi. Slim-llm: Saliency-driven mixed-precision quantization for large language models. *arXiv preprint arXiv:2405.14917*, 2024.
- Albert Q Jiang, Alexandre Sablayrolles, Antoine Roux, Arthur Mensch, Blanche Savary, Chris Bamford, Devendra Singh Chaplot, Diego de las Casas, Emma Bou Hanna, Florian Bressand, et al. Mixtral of experts. *arXiv preprint arXiv:2401.04088*, 2024.
- Jared Kaplan, Sam McCandlish, Tom Henighan, Tom B. Brown, Benjamin Chess, Rewon Child, Scott Gray, Alec Radford, Jeffrey Wu, and Dario Amodei. Scaling laws for neural language models, 2020.
- Shiro Kobayashi and Gerhard P Fettweis. A new approach for block-floating-point arithmetic. In *1999 IEEE International Conference on Acoustics, Speech, and Signal Processing. Proceedings. ICASSP99 (Cat. No. 99CH36258)*, volume 4, pp. 2009–2012. IEEE, 1999.
- Tanishq Kumar, Zachary Ankner, Benjamin F Spector, Blake Bordelon, Niklas Muennighoff, Manish Paul, Cengiz Pehlevan, Christopher Ré, and Aditi Raghunathan. Scaling laws for precision. *arXiv preprint arXiv:2411.04330*, 2024.
- Shiyao Li, Xuefei Ning, Ke Hong, Tengxuan Liu, Luning Wang, Xiuhong Li, Kai Zhong, Guohao Dai, Huazhong Yang, and Yu Wang. Llm-mq: Mixed-precision quantization for efficient llm deployment. In *The Efficient Natural Language and Speech Processing Workshop with NeurIPS*, volume 9, 2023.
- Wanchao Liang, Tianyu Liu, Less Wright, Will Constable, Andrew Gu, Chien-Chin Huang, Iris Zhang, Wei Feng, Howard Huang, Junjie Wang, Sanket Purandare, Gokul Nadathur, and Stratos Idreos. TorchTriton: One-stop pytorch native solution for production ready LLM pretraining. In *The Thirteenth International Conference on Learning Representations*, 2025. URL <https://openreview.net/forum?id=SFN6Wm7YBI>.
- Ji Lin, Jiaming Tang, Haotian Tang, Shang Yang, Wei-Ming Chen, Wei-Chen Wang, Guangxuan Xiao, Xingyu Dang, Chuang Gan, and Song Han. Awq: Activation-aware weight quantization for on-device llm compression and acceleration. *Proceedings of Machine Learning and Systems*, 6: 87–100, 2024.
- Lucas D Lingle. Transformer-vq: Linear-time transformers via vector quantization. *arXiv preprint arXiv:2309.16354*, 2023.
- Aixin Liu, Bei Feng, Bing Xue, Bingxuan Wang, Bochao Wu, Chengda Lu, Chenggang Zhao, Chengqi Deng, Chenyu Zhang, Chong Ruan, et al. Deepseek-v3 technical report. *arXiv preprint arXiv:2412.19437*, 2024a.
- Zechun Liu, Changsheng Zhao, Igor Fedorov, Bilge Soran, Dhruv Choudhary, Raghuraman Krishnamoorthi, Vikas Chandra, Yuandong Tian, and Tijmen Blankevoort. Spinqant: Llm quantization with learned rotations. *arXiv preprint arXiv:2405.16406*, 2024b.
- Anton Lozhkov, Loubna Ben Allal, Leandro von Werra, and Thomas Wolf. Fineweb-edu: the finest collection of educational content, 2024. URL <https://huggingface.co/datasets/HuggingFaceFW/fineweb-edu>.

- Naveen Mellempudi, Sudarshan Srinivasan, Dipankar Das, and Bharat Kaul. Mixed precision training with 8-bit floating point. *arXiv preprint arXiv:1905.12334*, 2019.
- Paulius Micikevicius, Sharan Narang, Jonah Alben, Gregory Diamos, Erich Elsen, David Garcia, Boris Ginsburg, Michael Houston, Oleksii Kuchaiev, Ganesh Venkatesh, et al. Mixed precision training. *arXiv preprint arXiv:1710.03740*, 2017.
- OpenAI. Openai gpt-4.5 system card. Technical report, OpenAI, February 2025.
- Yeonhong Park, Jake Hyun, SangLyul Cho, Bonggeun Sim, and Jae W Lee. Any-precision llm: Low-cost deployment of multiple, different-sized llms. *arXiv preprint arXiv:2402.10517*, 2024.
- Tim Pearce and Jinyeop Song. Reconciling kaplan and chinchilla scaling laws, 2024. URL <https://arxiv.org/abs/2406.12907>.
- Qwen Team. Qwen3 technical report. https://github.com/QwenLM/Qwen3/blob/main/Qwen3_Technical_Report.pdf, 2025. Accessed: 2025-05-14.
- Bitva Darvish Rouhani, Ritchie Zhao, Venmugil Elango, Rasoul Shafipour, Mathew Hall, Maral Mes-makhosroshahi, Ankit More, Levi Melnick, Maximilian Golub, Girish Varatkar, et al. Zhaoxia (summer) deng, sam naghshineh, jongsoo park, and maxim naumov. with shared microexponents, a little shifting goes a long way. In *Proceedings of the 50th Annual International Symposium on Computer Architecture, ISCA*, pp. 17–21, 2023.
- Wenqi Shao, Mengzhao Chen, Zhaoyang Zhang, Peng Xu, Lirui Zhao, Zhiqian Li, Kaipeng Zhang, Peng Gao, Yu Qiao, and Ping Luo. Omniquant: Omnidirectionally calibrated quantization for large language models. *arXiv preprint arXiv:2308.13137*, 2023.
- Daria Soboleva, Faisal Al-Khateeb, Robert Myers, Jacob R Steeves, Joel Hestness, and Nolan Dey. SlimPajama: A 627B token cleaned and deduplicated version of RedPajama. <https://www.cerebras.net/blog/slimpajama-a-627b-token-cleaned-and-deduplicated-version-of-redpajama>, 2023. URL <https://huggingface.co/datasets/cerebras/SlimPajama-627B>.
- Xiao Sun, Jungwook Choi, Chia-Yu Chen, Naigang Wang, Swagath Venkataramani, Vijayalakshmi Viji Srinivasan, Xiaodong Cui, Wei Zhang, and Kailash Gopalakrishnan. Hybrid 8-bit floating point (hfp8) training and inference for deep neural networks. *Advances in neural information processing systems*, 32, 2019.
- Ajay Tirumala and Raymond Wong. Nvidia blackwell platform: Advancing generative ai and accelerated computing. *2024 IEEE Hot Chips 36 Symposium*, pp. 1–33, 2024.
- Hugo Touvron, Louis Martin, Kevin Stone, Peter Albert, Amjad Almahairi, Yasmine Babaei, Nikolay Bashlykov, Soumya Batra, Prajjwal Bhargava, Shruti Bhosale, et al. Llama 2: Open foundation and fine-tuned chat models. *arXiv preprint arXiv:2307.09288*, 2023.
- Albert Tseng, Qingyao Sun, David Hou, and Christopher M De Sa. Qtip: Quantization with trellises and incoherence processing. *Advances in Neural Information Processing Systems*, 37:59597–59620, 2024.
- Xiuying Wei, Yunchen Zhang, Xiangguo Zhang, Ruihao Gong, Shanghang Zhang, Qi Zhang, Fengwei Yu, and Xianglong Liu. Outlier suppression: Pushing the limit of low-bit transformer language models. *Advances in Neural Information Processing Systems*, 35:17402–17414, 2022.
- Xiuying Wei, Yunchen Zhang, Yuhang Li, Xiangguo Zhang, Ruihao Gong, Jinyang Guo, and Xianglong Liu. Outlier suppression+: Accurate quantization of large language models by equivalent and optimal shifting and scaling. *arXiv preprint arXiv:2304.09145*, 2023.
- Guangxuan Xiao, Ji Lin, Mickael Seznec, Hao Wu, Julien Demouth, and Song Han. Smoothquant: Accurate and efficient post-training quantization for large language models. In *International Conference on Machine Learning*, pp. 38087–38099. PMLR, 2023.

- An Yang, Anfeng Li, Baosong Yang, Beichen Zhang, Binyuan Hui, Bo Zheng, Bowen Yu, Chang Gao, Chengen Huang, Chenxu Lv, et al. Qwen3 technical report. *arXiv preprint arXiv:2505.09388*, 2025.
- Shulin Zeng, Jun Liu, Guohao Dai, Xinhao Yang, Tianyu Fu, Hongyi Wang, Wenheng Ma, Hanbo Sun, Shiyao Li, Zixiao Huang, et al. Flightllm: Efficient large language model inference with a complete mapping flow on fpgas. In *Proceedings of the 2024 ACM/SIGDA International Symposium on Field Programmable Gate Arrays*, pp. 223–234, 2024.
- Cheng Zhang, Jianyi Cheng, Ilia Shumailov, George A Constantinides, and Yiren Zhao. Revisiting block-based quantisation: What is important for sub-8-bit llm inference? *arXiv preprint arXiv:2310.05079*, 2023a.
- Cheng Zhang, Jianyi Cheng, Zhewen Yu, and Yiren Zhao. Mase: An efficient representation for software-defined ml hardware system exploration. *Neurips Workshop Machine Learning for Systems 2023*, 2023b.
- Cheng Zhang, Jianyi Cheng, George A Constantinides, and Yiren Zhao. Lqer: Low-rank quantization error reconstruction for llms. *arXiv preprint arXiv:2402.02446*, 2024.
- Lancheng Zou, Wenqian Zhao, Shuo Yin, Chen Bai, Qi Sun, and Bei Yu. Bie: Bi-exponent block floating-point for large language models quantization. In *Forty-first International Conference on Machine Learning*, 2024.

A PRE-TRAINING CLM SERIES MODEL

As discussed in Section 3.1, we pre-trained a series of causal language models (CLMs) to facilitate our derivation of mixed quantization scaling laws and corresponding experiments, before we cross-validate our scaling laws on other open-source models.

Table 1: Model architecture of CLMs.

Model	Vocab size	Model dim	FFN dim	#Hidden layers	#Attention heads	#Key/value heads
60M	49152	384	1408	22	4	2
200M		768	2688	24	12	4
400M		960	3328	30	15	5
600M		1152	4096	32	18	6
1.1B		1536	5376	32	24	8

Model architecture and tokenizer We adopt the Llama-3 architecture, which incorporates group query attention (GQA) and rotary positional embedding (RoPE) (Dubey et al., 2024b). Table 1 summarizes the model architecture of our CLM series. We use HuggingFaceTB/cosmo2-tokenizer¹, an open-source tokenizer trained on 1M tokens and released by HuggingFace.

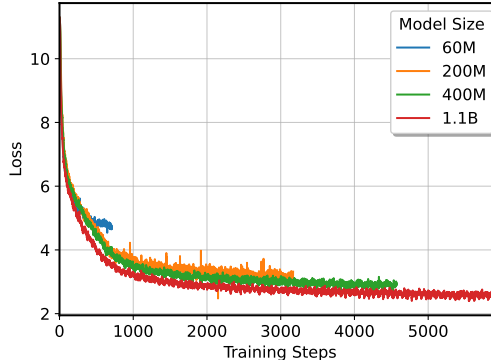


Figure 5: Pre-training loss of CLM series.

Pre-training setup We pre-train our models on FineWeb-Edu (Lozhkov et al., 2024), a pre-training dataset of cleaned and deduplicated english web data from CommonCrawl. We follow Chinchilla (Hoffmann et al., 2022) to determine the number of tokens for pre-training, *i.e.*, multiplying the number of parameters (without embedding layers) by 22. We use the AdamW optimizer with a linear learning rate schedule with 20% warmup. The initial learning rate is set to $1e-4$ and the sequence length is set to 2048. We use various batch sizes for different models, *i.e.*, 96 for 60M, 64 for 200M, 96 for 400M, 96 for 600M, and 192 for 1.1B. Figure 5 shows the pre-training loss of our CLM series. We will open-source our pre-trained models and tokenizer once the paper is accepted.

Pretraining framework We use TorchTitan (Liang et al., 2025), a PyTorch-based distributed training framework to pretrain our models. We apply fully sharded data parallel (FSDP) and gradient checkpointing to save GPU memory. Eight NVIDIA H200 GPUs were used for pre-training 600M and 1.1B models, and eight NVIDIA A100 GPUs were used for pre-training 60M, 200M, and 400M models. Before conducting the mixed quantization experiments, we convert the pre-trained models from torch distributed format to HuggingFace format.

¹cosmo2-tokenizer: <https://huggingface.co/HuggingFaceTB/cosmo2-tokenizer>

B DISTRIBUTION FOR SEARCH SPACE

Figure 6 present the kernel density estimates (KDEs) of the distribution Δ under MXINT-4 layerwise quantization, evaluated across varying numbers of trials: 100, 200, 500, and 1000. These KDEs are generated using a Gaussian kernel, which may not be the optimal kernel, providing a consistent and smooth estimate that is sufficient for comparative analysis.

We present Figures 6a to 6h, which shows the KDEs of different quantization ratios Q_r (from 0.5 to 0.8) for a fixed model (CLM-1.1B and CLM-200M), whereas Figures 6i to 6p shows the KDEs of different model sizes (from 60M to 600M) under fixed Q_r (0.5 and 0.6). Across all figures, as the sample size increases from 100 to 1000, the estimated distribution tends to remain the same. The KDEs generated appear nearly indistinguishable in shape from that of 100. This consistency holds throughout different Q_r and model sizes.

These figures suggest that the empirical distribution of Δ can be reliably estimated with as few as 100 samples, as presented in Section 3.1. That is, even with relatively small sample sizes, the mean ($\mathbb{E}(\Delta)$) and minimum (δ^{opt}) values of Δ can still be well captured. Therefore, from both a computational and statistical efficiency perspective, excessive sampling provides diminishing returns. This insight is particularly valuable since large-scale sampling is computationally expensive.

C LAYER-WISE RESULTS

As shown in Section 3, Figure 7 and Figure 8 show the actual and fitted loss contour of CLM, Qwen1.5, and Qwen3 under MXINT4 layerwise quantization. For each model family we present two contours: loss versus model size N and loss versus quantization ratio Q_r . Figure 7 shows the contour for the minimum value δ^{opt} and Figure 8 shows the expectation value δ_μ . There are a few outliers that do not match our fitted contour, which could be caused by the instability of the sampling process. In addition, note that the actual losses themselves are estimations.

D MATRIX MULTIPLICATION-WISE RESULTS

Following the layer-wise results in Section 3, the matrix multiplication-wise with Figure 9 and Figure 10 shows the actual and fitted loss contour of CLM, Qwen-1.5, and Qwen-3 under MXINT-4 matrix multiplication-wise quantization. For each model family, we present two contours: loss versus model size N and loss versus quantization ratio Q_r . Figure 9 shows the contour for the minimum value δ^{opt} and Figure 10 shows the expectation value δ_μ . As with the layer-wise quantization results, a few outliers deviate from the fitted contours due to the variability in the sampling process.

While Figure 9 and Figure 10 show the effectiveness of the weak law, Figure 11, Figure 12, and Figure 13 demonstrate the utility for the strong law. Those three figures show the actual and fitted loss contours (both minimum and mean) with respect to block size Q_b with different quantization ratios Q_r for CLM, Qwen-1.5, and Qwen-3. For those figures, our strong law only takes into consideration losses that are less than 100, since larger losses in perplexity are meaningless under our setting (in practical term, these models would not generate anything distinguishable). As a result, the fitted contours are not accurate when the actual loss is large, which is acceptable since we do not care about those excessive losses.

E OTHER NUMERICAL FORMAT RESULTS

Figures 14 and 15 present the minimum and mean loss contours with respect to model size N and quantization ratio Q_r for the CLM, Qwen-1.5, and Qwen-3 models under HQQ quantization. These results demonstrate that HQQ is a highly effective quantization method, successfully preserving the capabilities of the pre-trained models and maintaining low post-training quantization (PTQ) loss. Notably, the fitted contours closely match the empirical data across all model families, indicating that our scaling law formulation generalizes well, even under high-performance quantization methods.

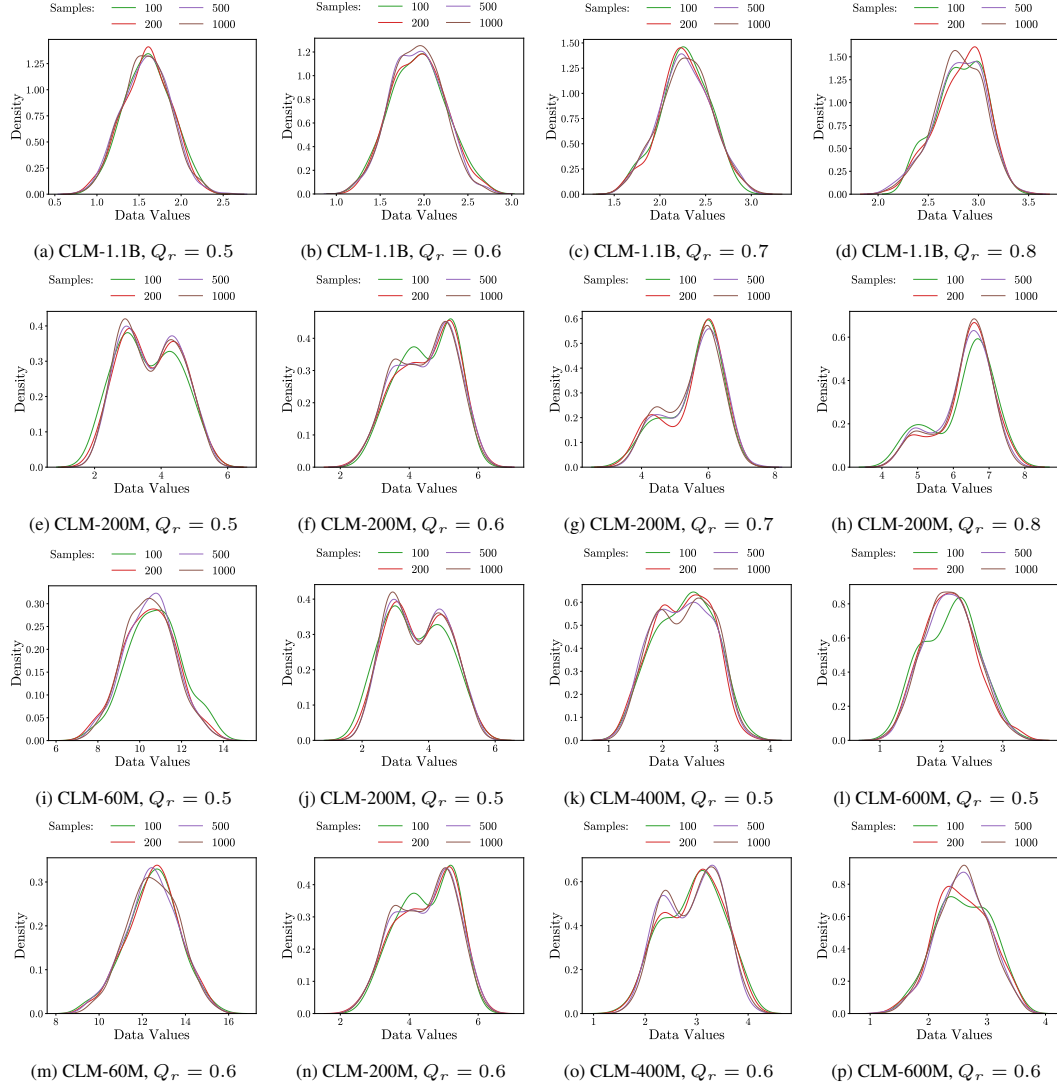


Figure 6: **KDE of distribution Δ .** Different KDE for different Q_r under a fixed models: (a,b,c,d) Changing Q_r for CLM-1.1B; (e,f,g,h) Changing Q_r for CLM-200M. KDE for different model under fixed Q_r ; (i,j,k,l) Changing N for $Q_r = 0.5$; (m,n,o,p) Changing N for $Q_r = 0.6$.

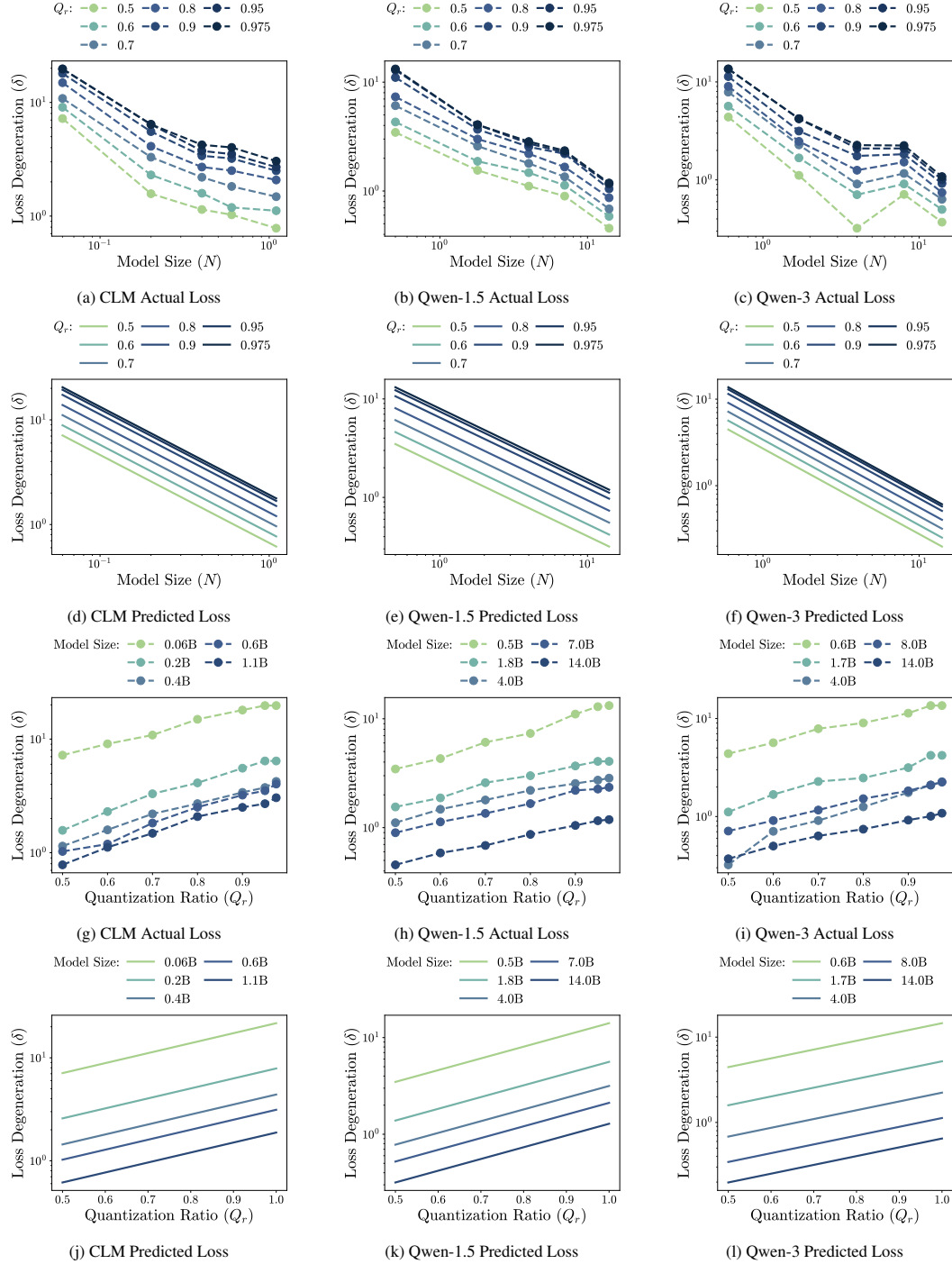


Figure 7: **Layer-wise** (δ^{opt}) (a,d,g,h) CLM layer-wise results; (b,e,h,k) Qwen-1.5 layer-wise results; (c,f,i,l) Qwen-3 layer-wise results.

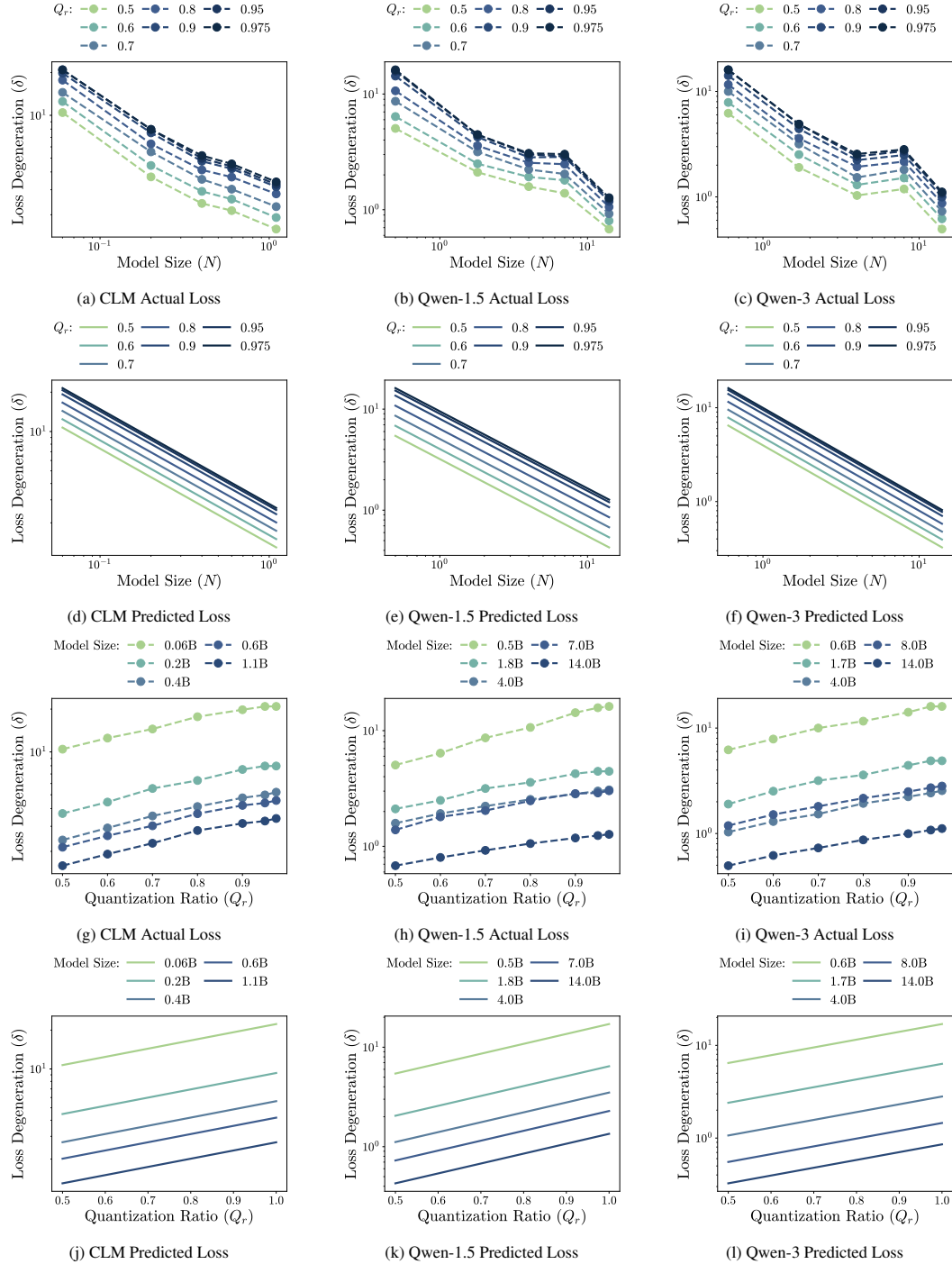


Figure 8: **Layer-wise** (δ_μ) (a,d,g,h) CLM layer-wise results; (b,e,h,k) Qwen-1.5 layer-wise results; (c,f,i,l) Qwen-3 layer-wise results.

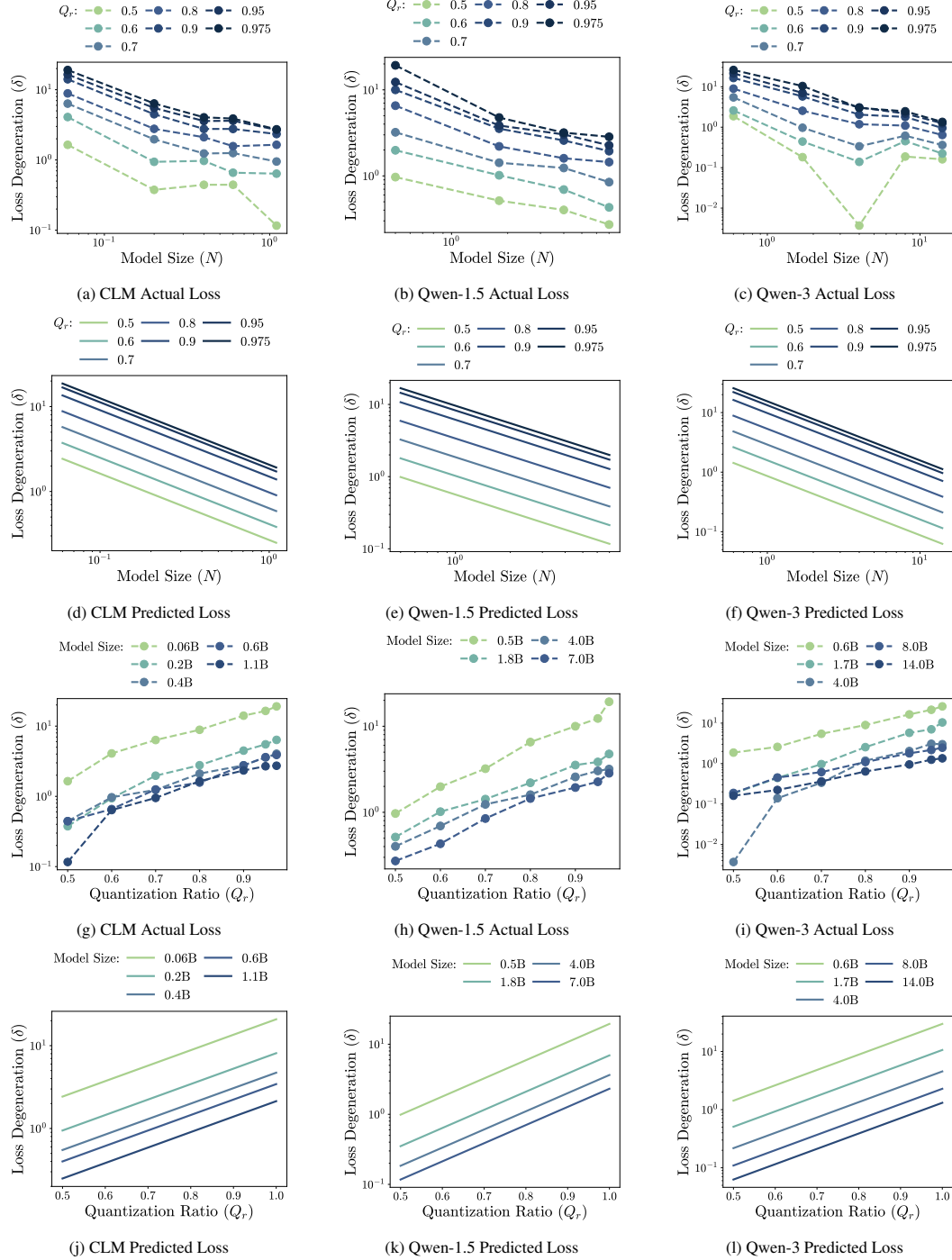


Figure 9: **Matrix Multiplication-wise (δ^{opt})** (a,d,g,h) CLM matrix multiplication-wise results; (b,e,h,k) Qwen-1.5 matrix multiplication-wise results; (c,f,i,l) Qwen-3 matrix multiplication-wise results.

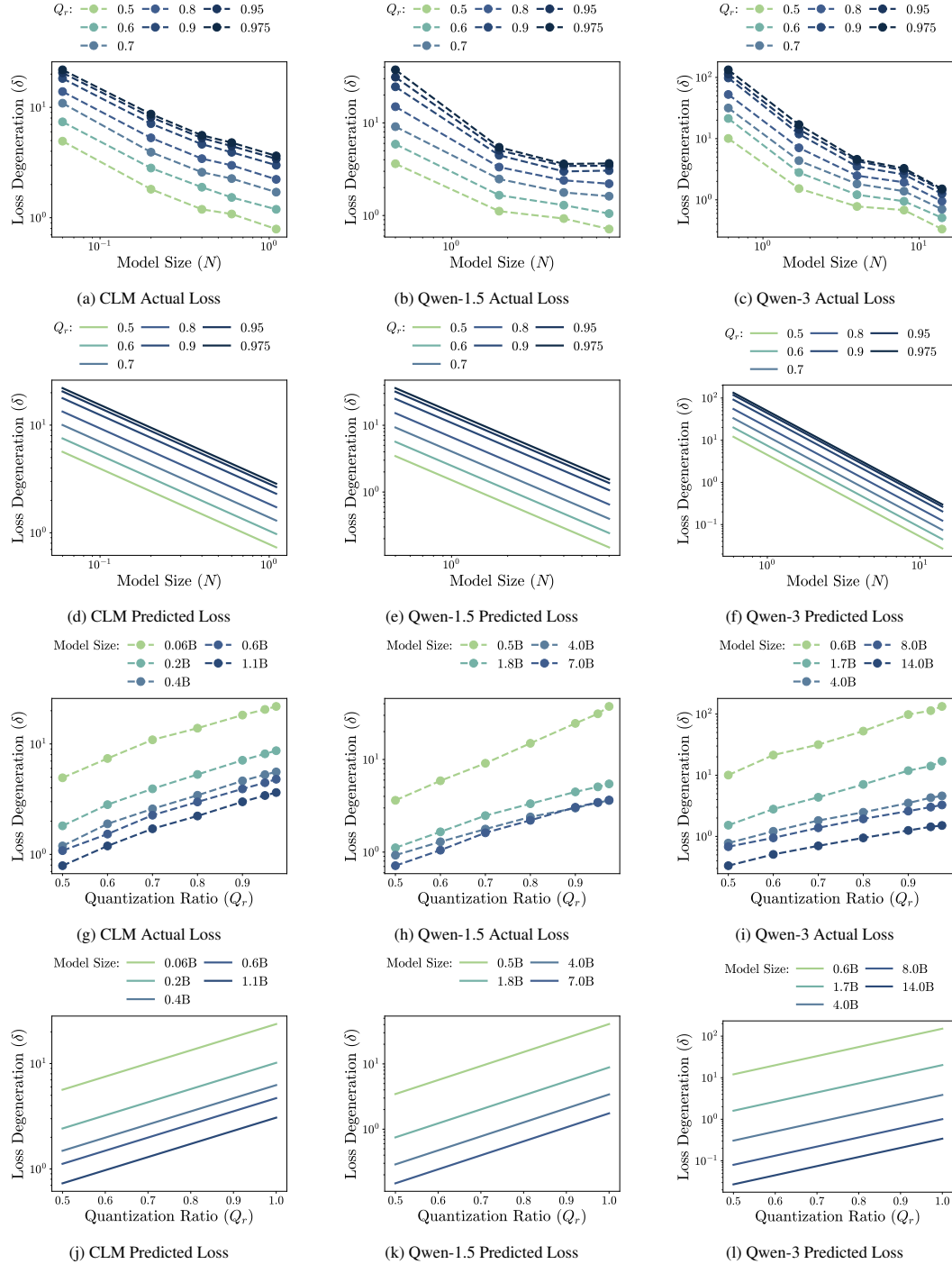


Figure 10: **Matrix Multiplication-wise** (δ_μ) (a,d,g,h) CLM matrix multiplication-wise results; (b,e,h,k) Qwen-1.5 matrix multiplication-wise results; (c,f,i,l) Qwen-3 matrix multiplication-wise results.

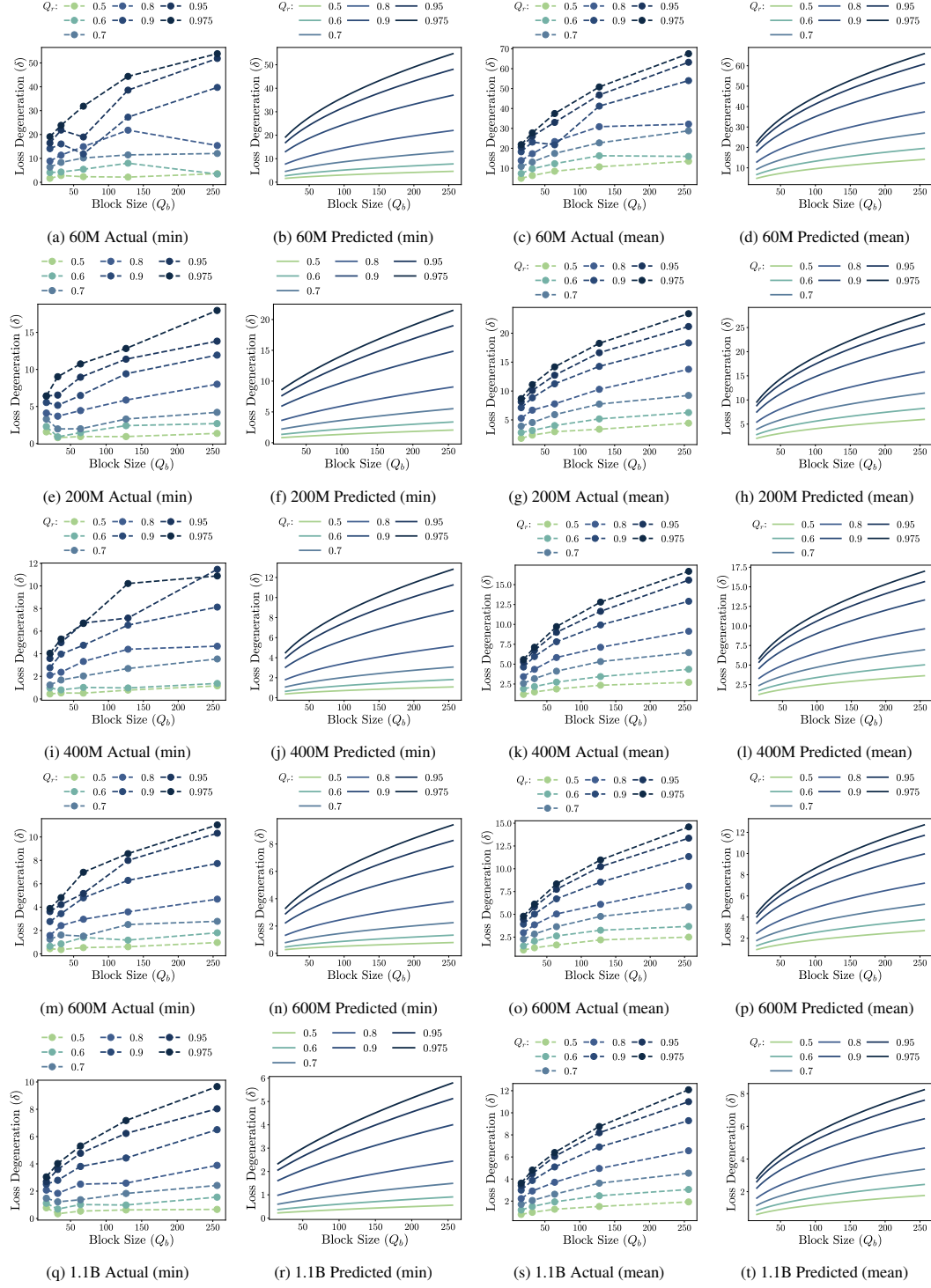


Figure 11: **Strong Law CLM Matrix Multiplication-wise** (δ^{opt} , δ_{μ}) (a,b,e,f,i,j,m,n,q,r) CLM matrix multiplication-wise δ^{opt} results; (c,d,g,h,k,l,o,p,s,t) CLM matrix multiplication-wise δ_{μ} results.

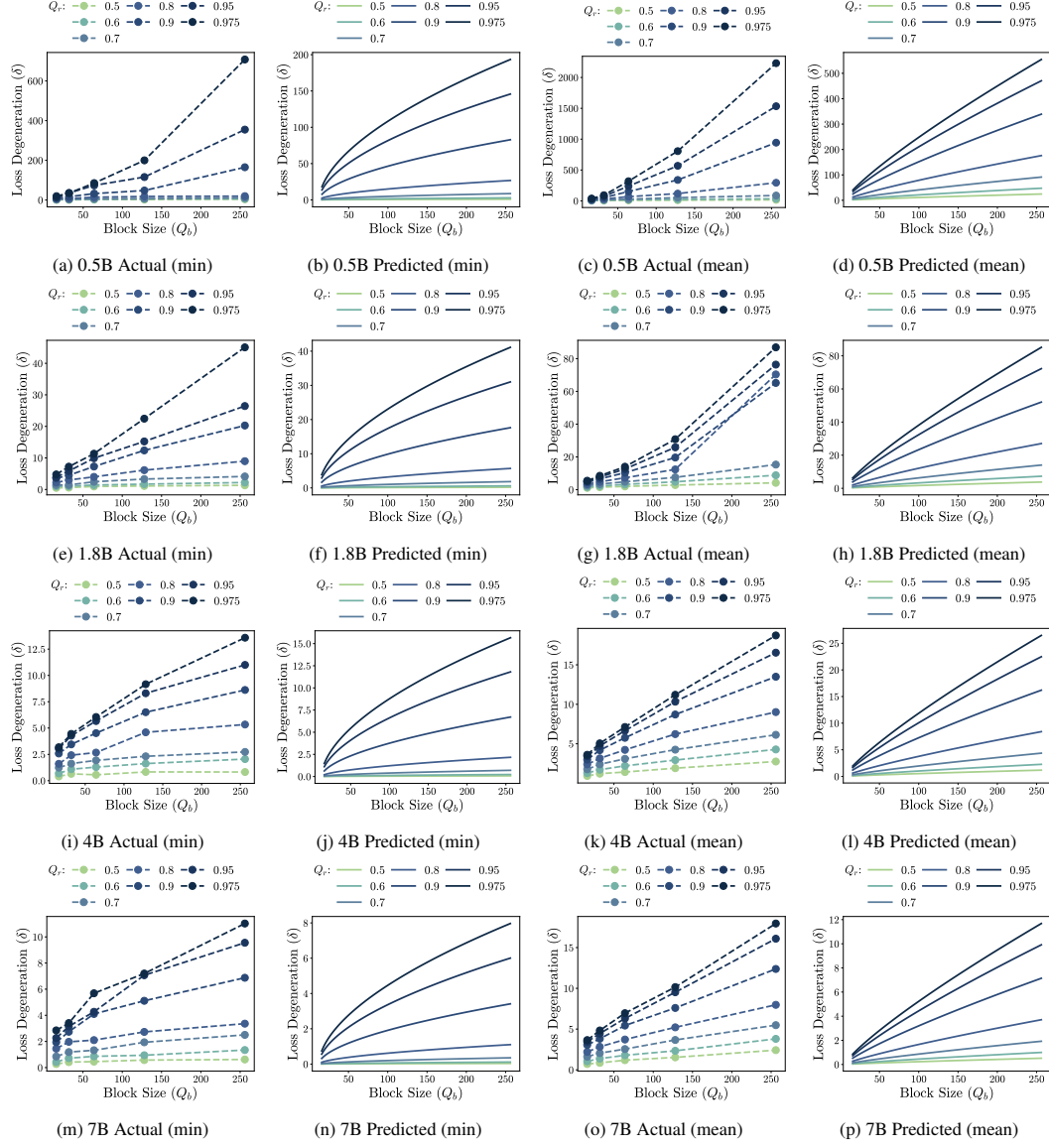


Figure 12: **Strong Law Qwen-1.5 Matrix Multiplication-wise** (δ^{opt} , δ_μ) (a,b,e,f,i,j,m,n) Qwen1.5 matrix multiplication-wise δ^{opt} results; (c,d,g,h,k,l,o,p) Qwen1.5 matrix multiplication-wise δ_μ results.

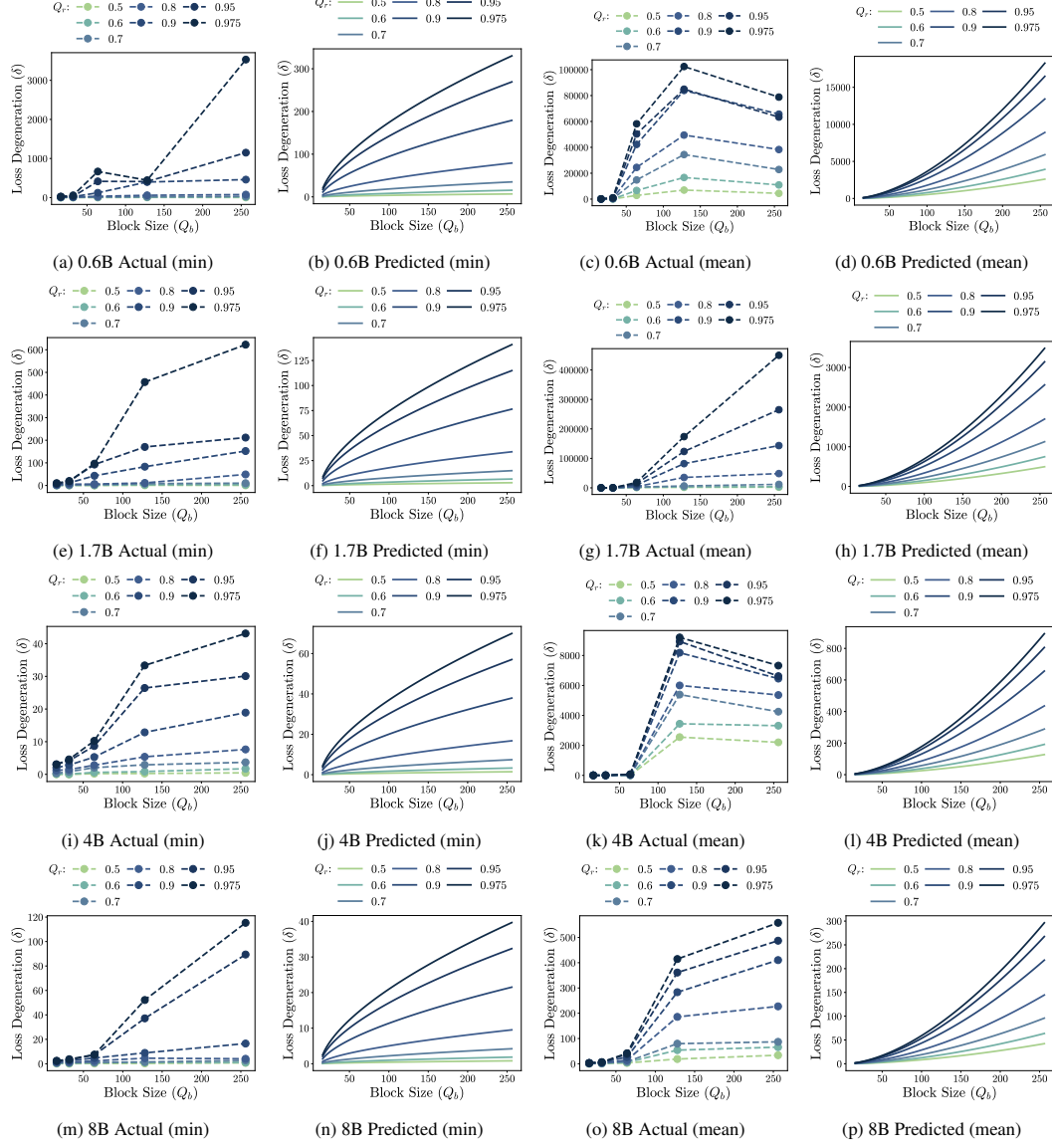


Figure 13: **Strong Law Qwen-3 Matrix Multiplication-wise** (δ^{opt} , δ_μ) (a,b,e,f,i,j,m,n) Qwen3 matrix multiplication-wise δ^{opt} results; (c,d,g,h,k,l,o,p) Qwen3 matrix multiplication-wise δ_μ results.

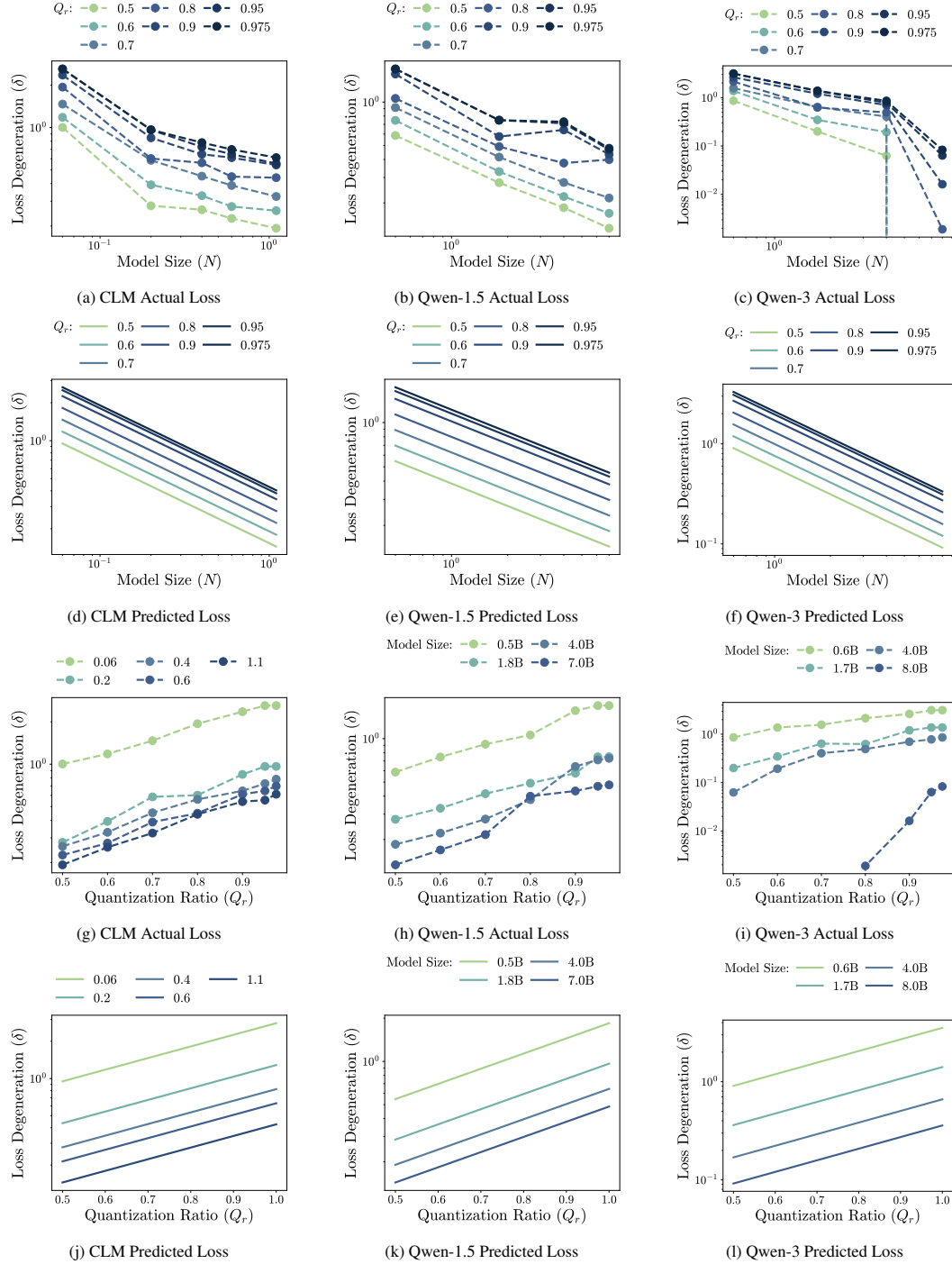


Figure 14: **HQQ** (δ^{opt}) (a,d,g,h) CLM HQQ results; (b,e,h,k) Qwen-1.5 HQQ results; (c,f,i,l) Qwen-3 HQQ results.

Note that, under these settings, there are some significant outliers for Qwen-3 results, with negative PTQ losses, such negative PTQ losses might be caused by the fact that *all Qwen-3 models involved in our experiments are partially distilled from larger models* as indicated in (Yang et al., 2025), invalidating our assumptions in Section 2.

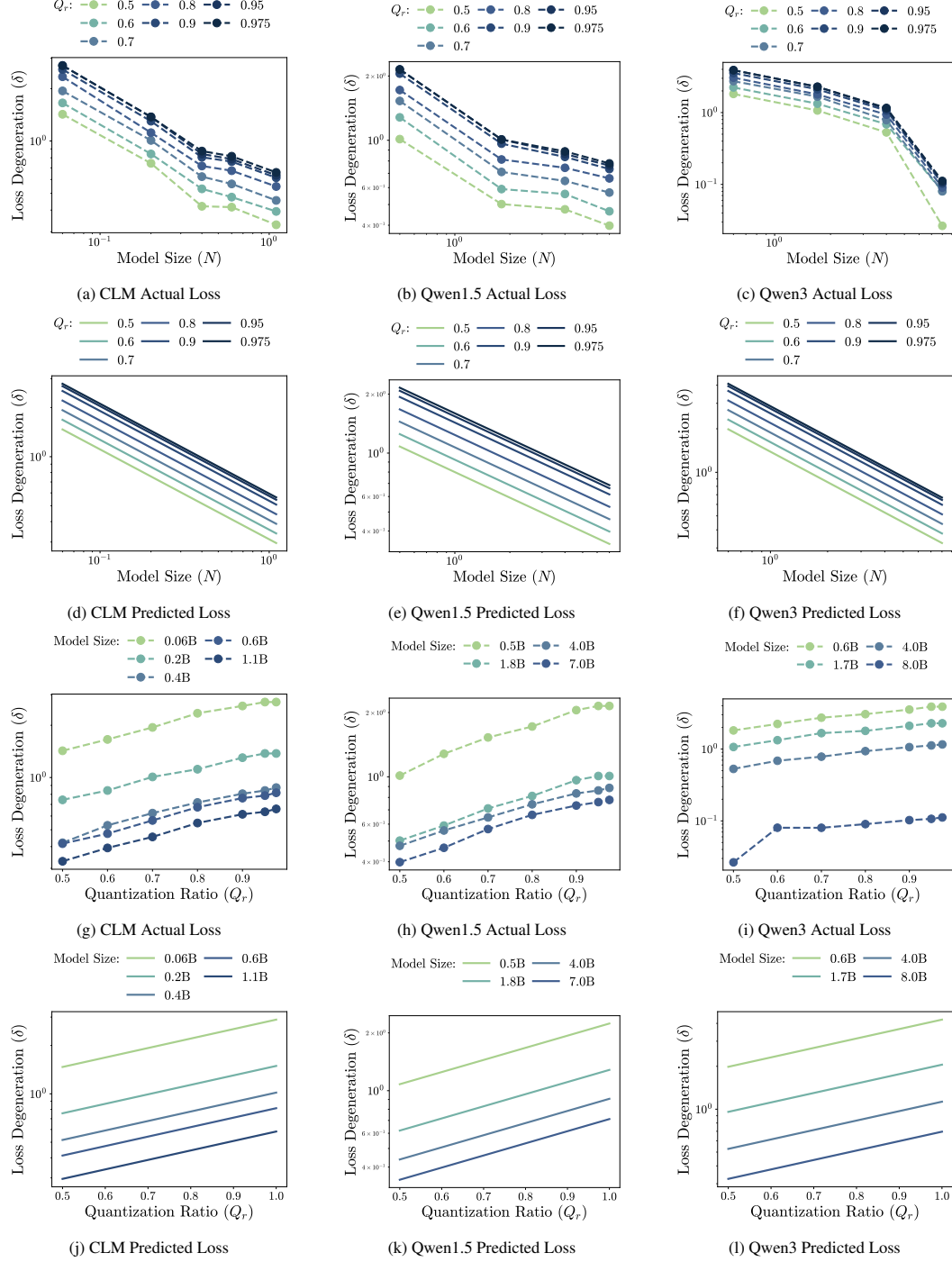


Figure 15: **HQQ** (δ_μ) (a,d,g,h) CLM HQQ results; (b,e,h,k) Qwen-1.5 HQQ results; (c,f,i,l) Qwen-3 HQQ results.

In contrast, Figures 16 and 17 show the results for MXINT-2 quantization, which performs poorly across the board. The loss increases significantly under this setting, suggesting that aggressive quantization in both weights and activations severely degrades model quality. Despite the high loss, our fitted contours remain aligned with the empirical observations, capturing the underlying loss surface accurately.

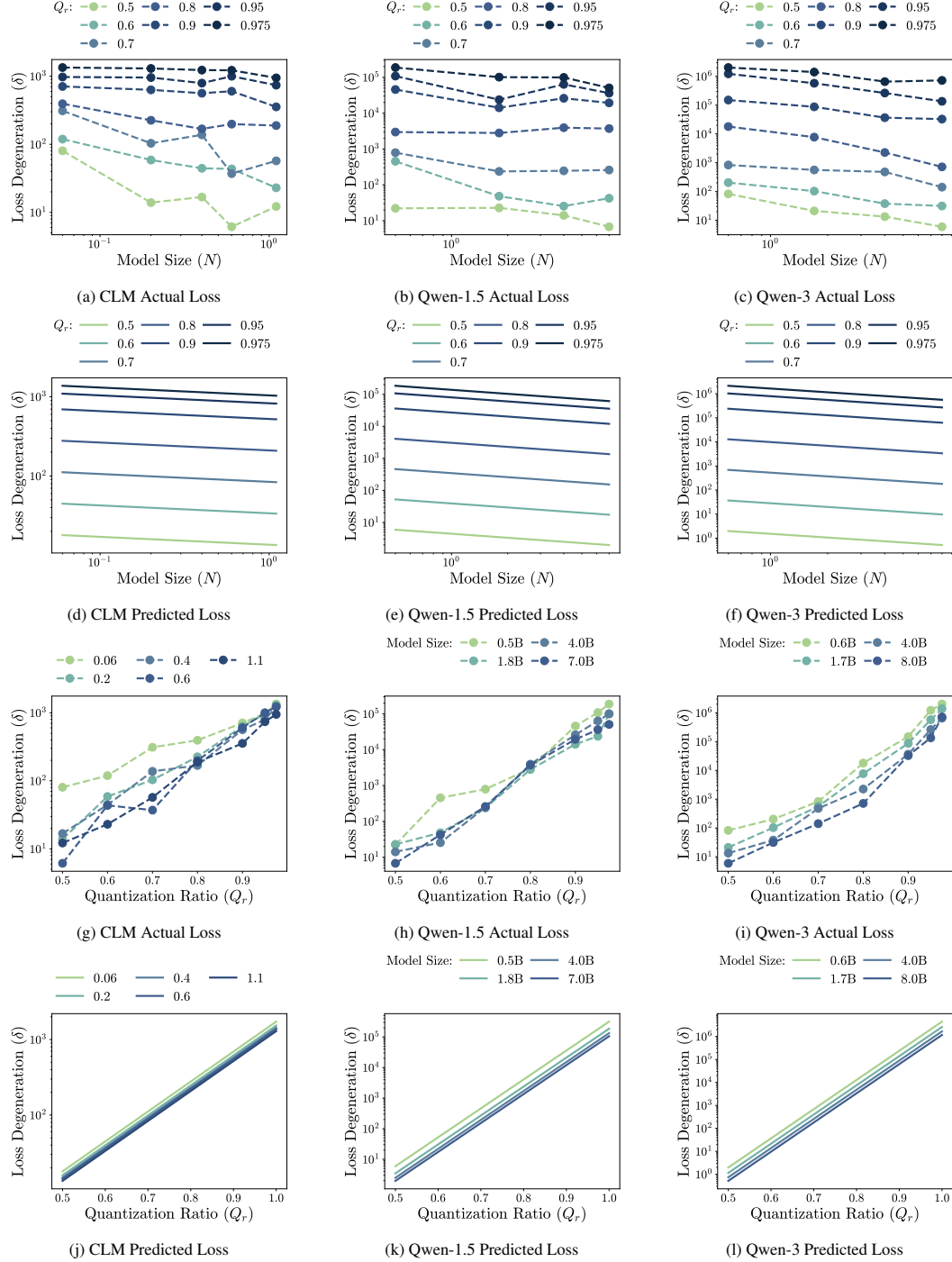


Figure 16: MXINT-2 (δ^{opt}) (a,d,g,h) CLM MXINT-2 results; (b,e,h,k) Qwen-1.5 MXINT-2 results; (c,f,i,l) Qwen-3 MXINT-2 results.

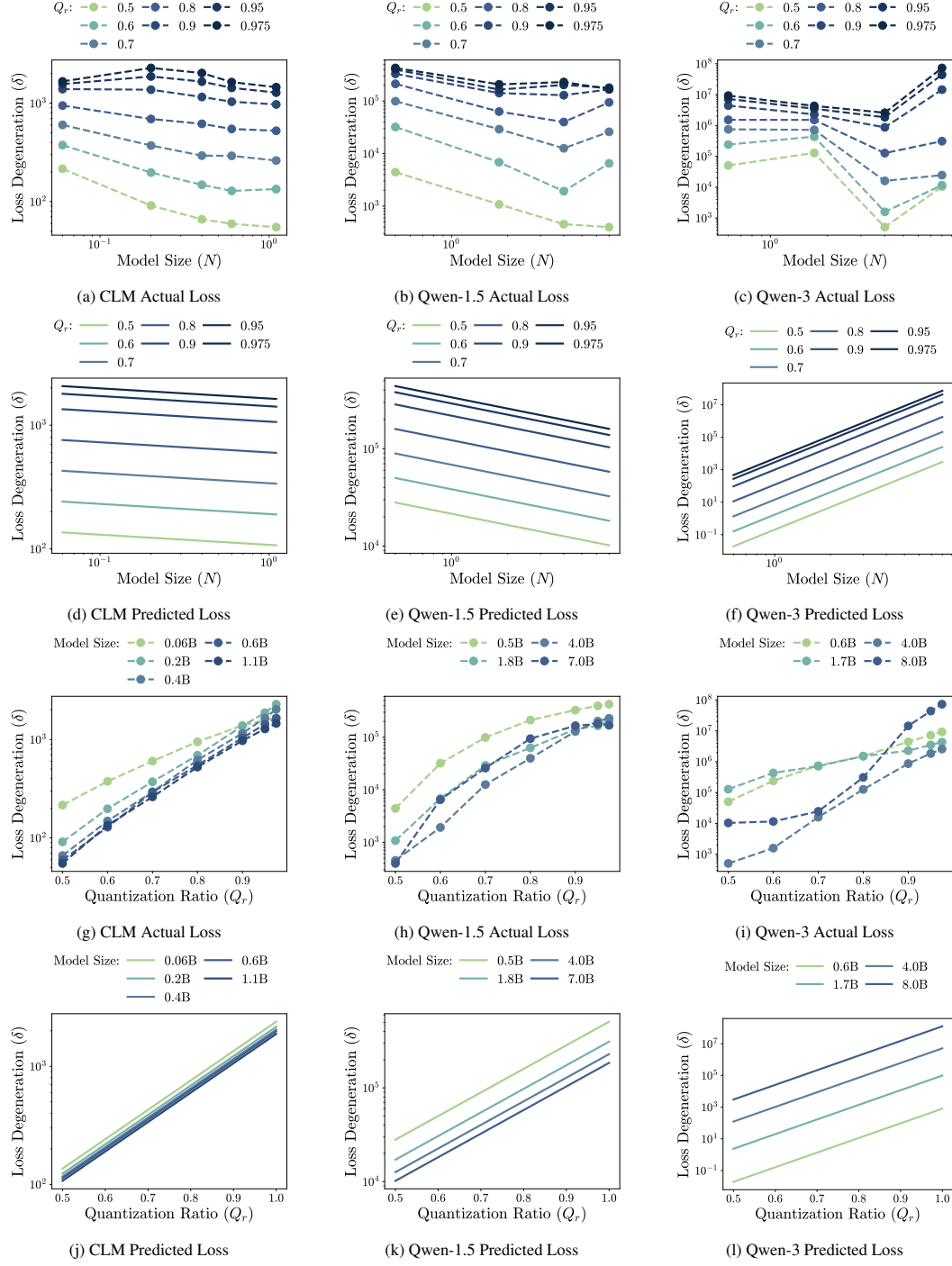


Figure 17: **MXINT-2** (δ_μ) (a,d,g,h) CLM MXINT2 results; (b,e,h,k) Qwen-1.5 MXINT2 results; (c,f,i,l) Qwen-3 MXINT2 results.

Figures 18 and 19 display the loss contours for MXINT-4 weight-only quantization. This method shows moderate performance. It incurs a smaller degradation in loss than MXINT-2. The fitted contours once again align well with actual measurements, reinforcing the robustness of our scaling law across varying quantization granularities and levels of aggressiveness. Similar to the HQQ quantization, the effectiveness of MXINT-4 weight-only quantization and the distillation training process of Qwen-3 explains the outliers for Qwen-3 figures.

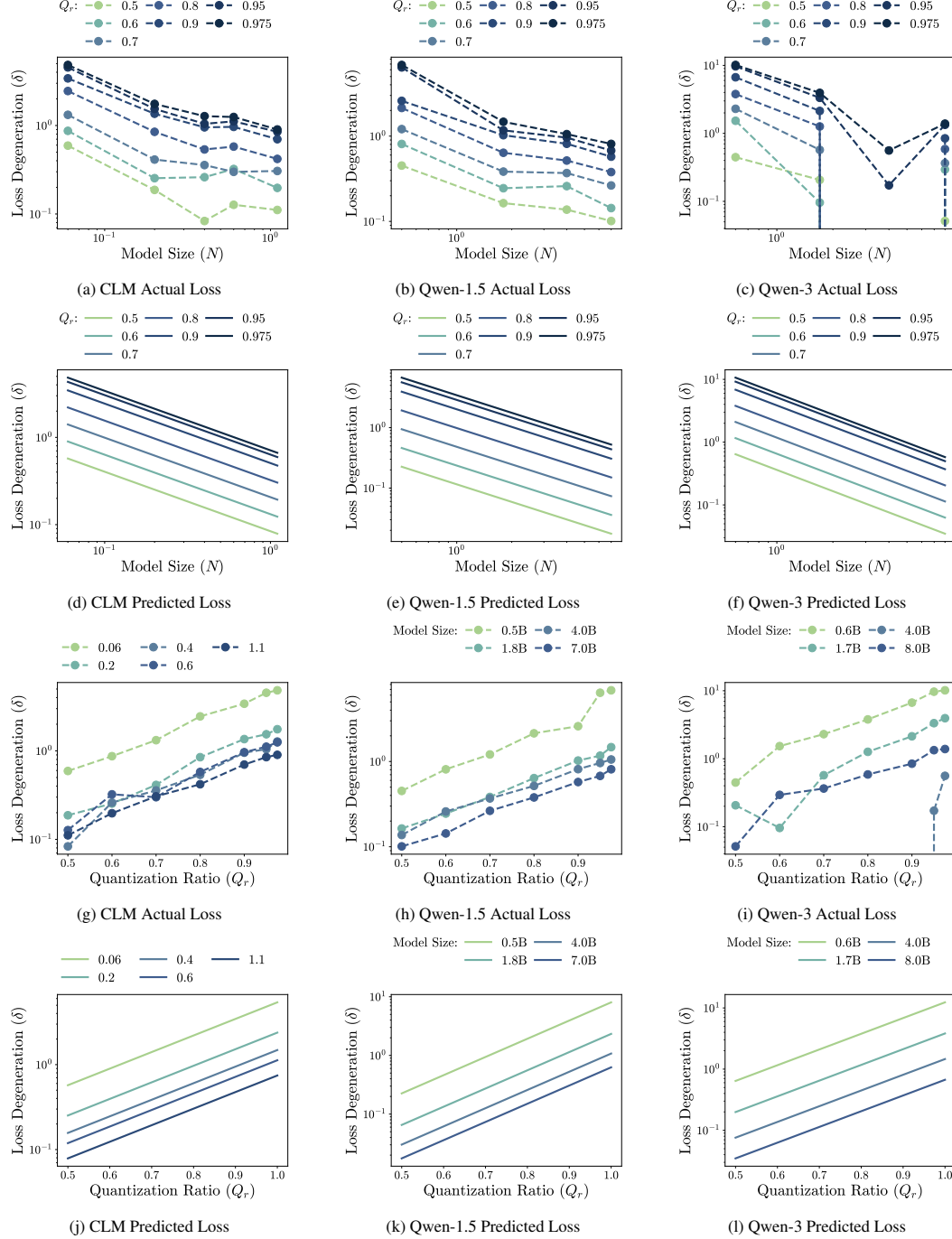


Figure 18: **MXINT-4 Weight-only** (δ^{opt}) (a,d,g,h) CLM MXINT-4 Weight-only results; (b,e,h,k) Qwen-1.5 MXINT4 Weight-only results; (c,f,i,l) Qwen-3 MXINT-4 Weight-only results.

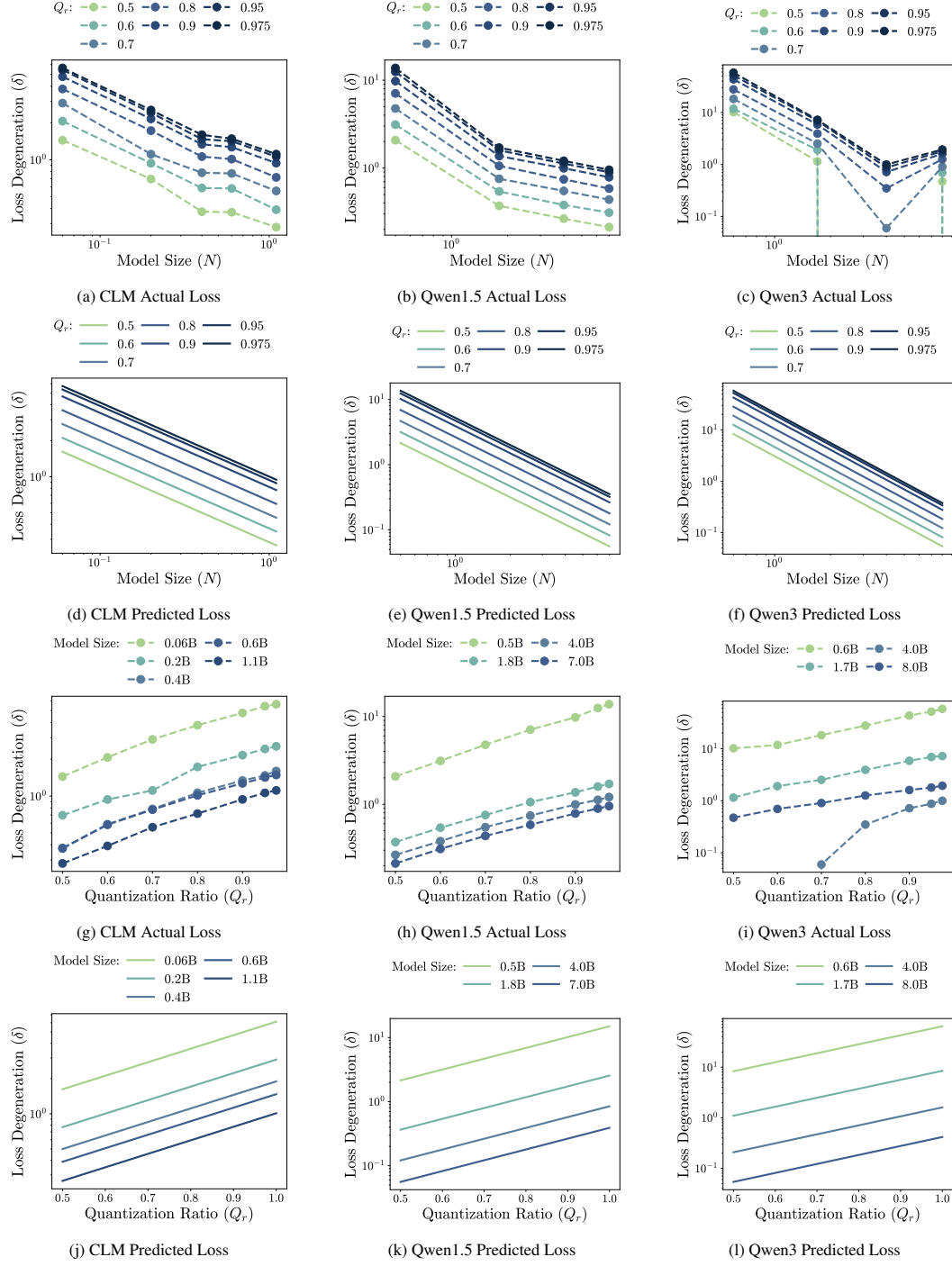


Figure 19: **MXINT4 Weight-only (δ_μ)** (a,d,g,h) CLM MXINT4 Weight-only results; (b,e,h,k) Qwen-1.5 MX-INT4 Weight-only results; (c,f,i,l) Qwen-3 MXINT4 Weight-only results.

F FORMULA FITTING

We report all fitted coefficients and R^2 plots in Figures 20 to 37. These include block-wise strong law fittings, as well as weak law fittings under layerwise, matrix-multiplication-wise, HQQ, MXINT2, and MXINT4 weight-only quantization. Each table reports the coefficients described in Section 2 from our scaling law equations, and the scatter plots compare predicted and actual PTQ losses to evaluate the fitting quality.

Overall Trends and Implications. Across all quantization levels and model families, the R^2 plots validate the predictive power of our scaling laws. Tight clustering along the diagonal confirms that the fitted models not only approximate empirical losses well but also generalize across compression levels and model sizes. Exceptions, including negative γ_N or inflated constants, indicate model-instability or ill-posed settings such as distillation pre-training or over-compression.

Block-wise Strong Law Fitting Figures 20–22 display the strong law fits across model families. For CLM and Qwen1.5, we observe high-quality fits with consistent scaling exponents. However, Qwen3 shows greater variability, with large γ_c values (e.g., 1.67), indicating strong sensitivity to the quantization ratio Q_r , likely caused by its distillation-only training pipeline.

Layerwise and Matrix Multiplication-wise MXINT-4 Fitting Figures 29–34 show the layerwise and matrix multiplication-wise MXINT4 quantization weak law results in strong, consistent fits across CLM and Qwen-1.5.

HQQ Fitting Figures 23–25 demonstrate that HQQ quantization maintains consistently good fits across all model families. These weak law results further confirm the strength of HQQ in preserving model accuracy after quantization, and they validate that our scaling law generalizes even under high-performance quantizers.

MXINT-2 Fitting Figures 26–28 illustrate that MXINT2—our most aggressive quantization—yields degraded fits. This is especially evident for Qwen-1.5, where fitted constants reach extreme values (e.g., $C = 1181.1$), and for Qwen-3, where γ_N becomes negative (-4.62), indicating that MXINT-2 quantization is not ideal. Despite this, the R^2 plots still show approximate alignment, suggesting that the weak law scaling structure is partially preserved.

MXINT-4 Weight-only Fitting Figures 35–37 confirm that weight-only MXINT-4 quantization achieves a balanced tradeoff: it reduces parameter precision with less impact on performance compared to MXINT2. Fit quality remains strong with reasonable coefficients. These trends validate that restricting quantization to weights alone preserves much of the original loss landscape structure, and our weak law accurately tracks this behavior across CLM, Qwen-1.5, and Qwen-3.

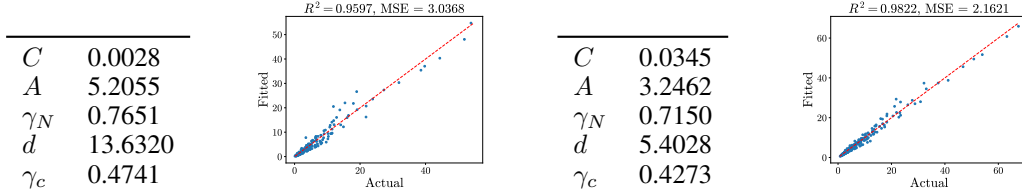
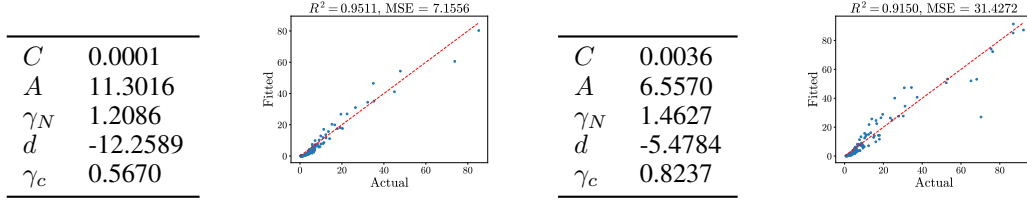
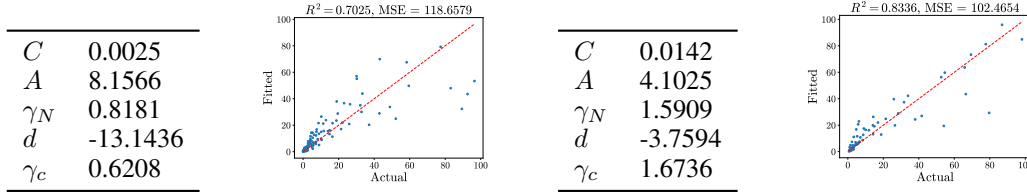
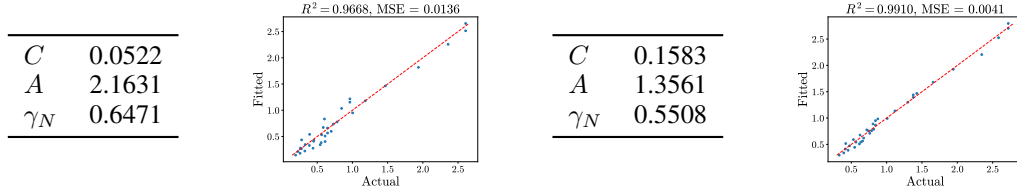
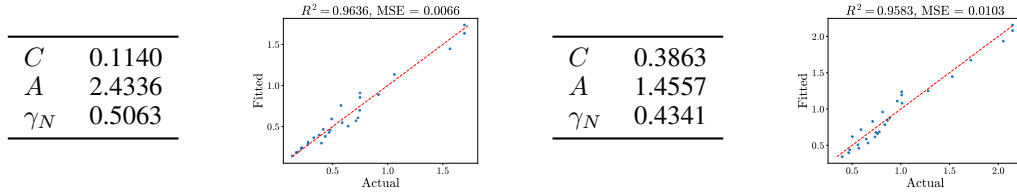
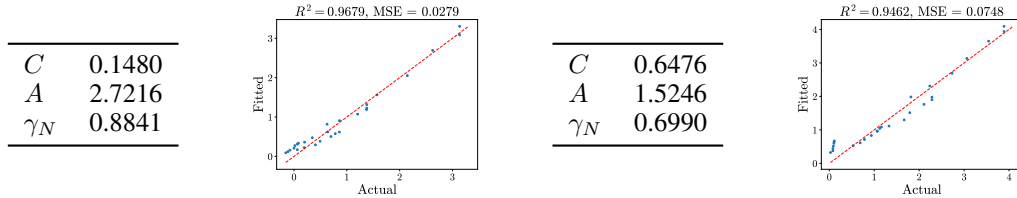
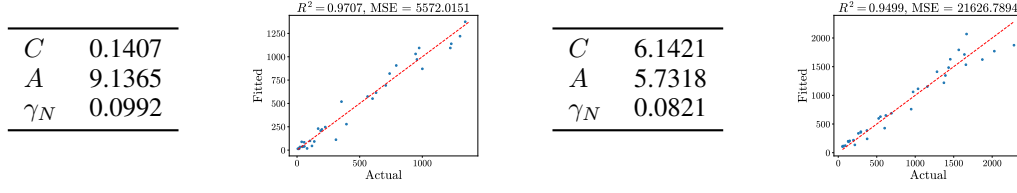
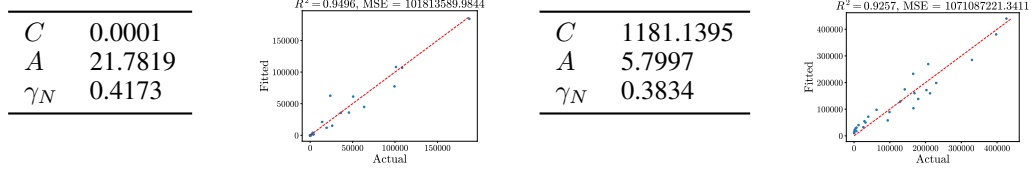
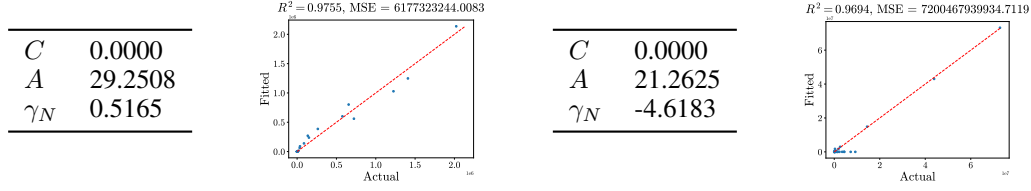
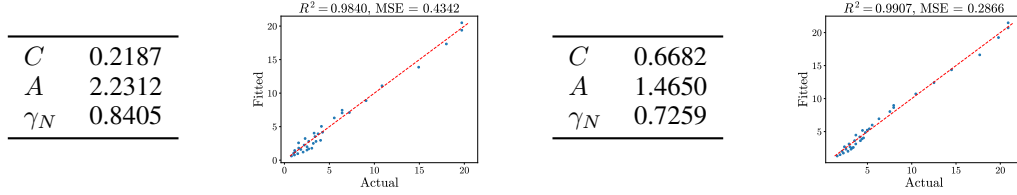
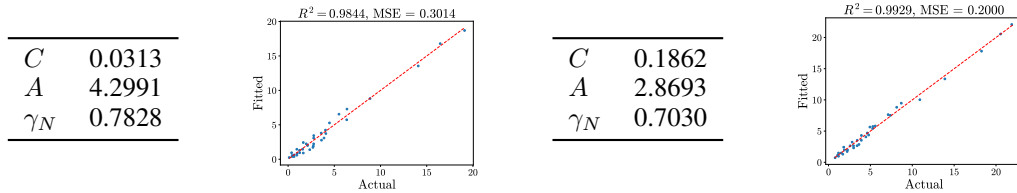
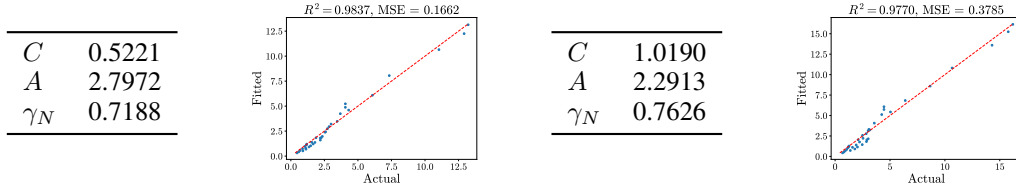
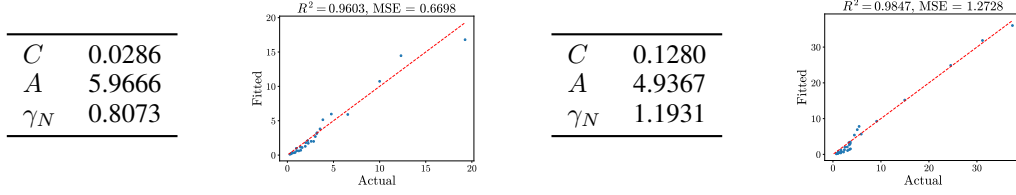
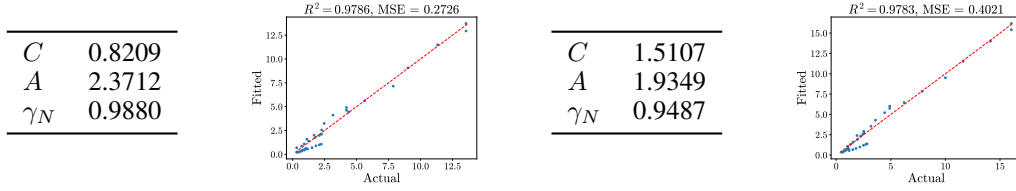
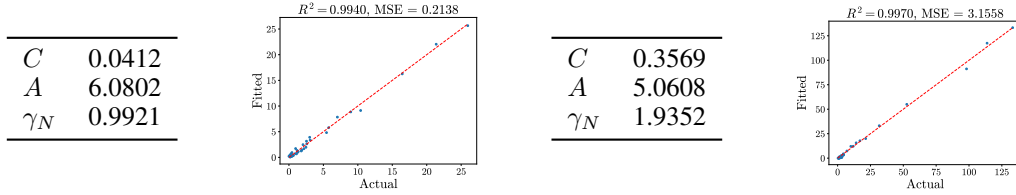
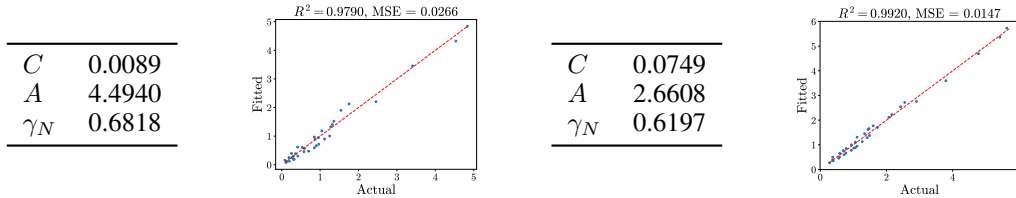


Figure 20: **CLM Strong Law.** The left two are for δ^{opt} and The right two are for δ_μ

Figure 21: **Qwen-1.5 Strong Law.** The left two are for δ^{opt} and The right two are for δ_μ Figure 22: **Qwen-3 Strong Law.** The left two are for δ^{opt} and The right two are for δ_μ Figure 23: **HQQ CLM Weak Law.** The left two are for δ^{opt} and The right two are for δ_μ Figure 24: **HQQ Qwen-1.5 Weak Law.** The left two are for δ^{opt} and The right two are for δ_μ Figure 25: **HQQ Qwen-3 Weak Law.** The left two are for δ^{opt} and The right two are for δ_μ

Figure 26: **MXINT-2 CLM Weak Law.** The left two are for δ^{opt} and The right two are for δ_μ Figure 27: **MXINT-2 Qwen-1.5 Weak Law.** The left two are for δ^{opt} and The right two are for δ_μ Figure 28: **MXINT-2 Qwen-3 Weak Law.** The left two are for δ^{opt} and The right two are for δ_μ Figure 29: **MXINT-4 Layerwise CLM Weak Law.** The left two are for δ^{opt} and The right two are for δ_μ Figure 30: **MXINT-4 Matrix Multiplication-wise CLM Weak Law.** The left two are for δ^{opt} and The right two are for δ_μ

Figure 31: **MXINT-4 Layerwise Qwen-1.5 Weak Law.** The left two are for δ^{opt} and The right two are for δ_μ Figure 32: **MXINT-4 Matrix Multiplication-wise Qwen-1.5 Weak Law.** The left two are for δ^{opt} and The right two are for δ_μ Figure 33: **MXINT-4 Layerwise Qwen-3 Weak Law.** The left two are for δ^{opt} and The right two are for δ_μ Figure 34: **MXINT-4 Matrix Multiplication-wise Qwen-3 Weak Law.** The left two are for δ^{opt} and The right two are for δ_μ Figure 35: **Weight-only MXINT-4 CLM Weak Law.** The left two are for δ^{opt} and The right two are for δ_μ

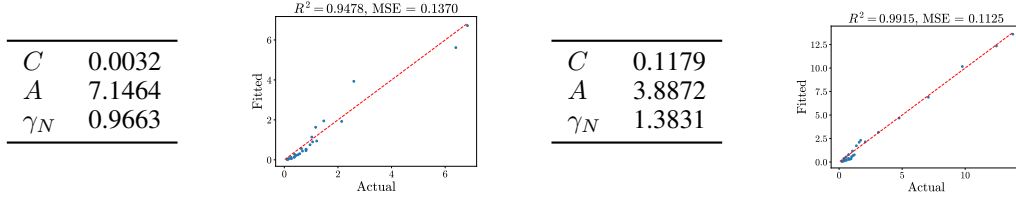


Figure 36: **Weight-only MXINT-4 Qwen-1.5 Weak Law.** The left two are for δ^{opt} and The right two are for δ_μ

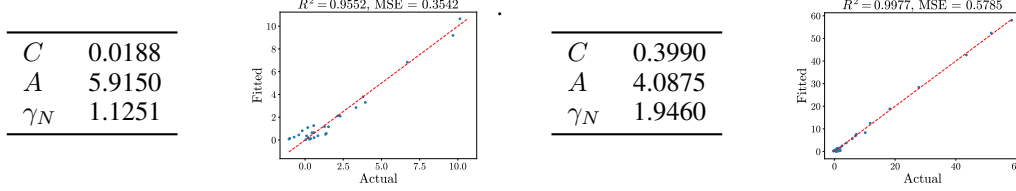


Figure 37: **Weight-only MXINT-4 Qwen-3 Weak Law.** The left two are for δ^{opt} and The right two are for δ_μ

G FURTHER EXPLANATION FOR OUR ESTIMATION OF $\mathbb{E}(\Delta)$ AND $\min(\Delta)$

As discussed in Section 2, we are interested in two parameters of the discrete random variable Δ : $\mathbb{E}(\Delta)$ and $\min(\Delta)$, which represent the mean and minimum (optimal) values of Δ . In the weak law, they are denoted as $\delta^{\text{opt}}(N, Q_r)$ and $\mathbb{E}[\Delta(N, Q_r)]$. In the strong law, they are denoted as $\delta^{\text{opt}}(N, Q_r, Q_b)$ and $\mathbb{E}[\Delta(N, Q_r, Q_b)]$.

We estimate those two parameters with the following two estimator. Given a list of i.i.d. discrete random variables $\{\Delta_i\}_{i=1}^n$. We denote the unbiased estimator of $\mathbb{E}(\Delta)$ as

$$E_n = \frac{\sum_{i=1}^n \Delta_i}{n}, \quad (20)$$

and the biased estimator of $\min(\Delta)$ as

$$M_n = \min(\{\Delta_i : i = 1, \dots, n\}). \quad (21)$$

E_n is an unbiased estimator as

$$\begin{aligned} \mathbb{E}(E_n) - \mathbb{E}(\Delta) &= \frac{\sum_{i=1}^n \mathbb{E}(\Delta_i)}{n} - \mathbb{E}(\Delta) \\ &= \mathbb{E}(\Delta) - \mathbb{E}(\Delta) \\ &= 0. \end{aligned} \quad (22)$$

On the other hand, M_n is a biased estimator. Without loss of generality, we will calculate the bias of $M'_n = \max(\{\Delta_i : i = 1, \dots, n\})$ with respect to $\max(\Delta)$. Since $\{\Delta_i\}_{i=1}^n$ are i.i.d,

$$\begin{aligned} \Pr(M'_n < x) &= \prod_{i=1}^n \Pr(\Delta_i < x) \\ &= F^n(x^-), \end{aligned} \quad (23)$$

where F is the cdf of Δ and $x^- = \max(\{x' : x' < x \wedge \Pr(\Delta = x') \neq 0\} \cup -\infty)$. Hence the expectation of M'_n is

$$\begin{aligned} \mathbb{E}(M'_n) &= \sum_x x \Pr(M'_n = x) \\ &= \sum_x x \Pr(M'_n \leq x \wedge M'_n \not\leq x) \\ &= \sum_x x(F^n(x) - F^n(x^-)). \end{aligned} \quad (24)$$

As

$$\sum_x (F^n(x) - F^n(x^-)) = F^n(\max(\Delta)) - F^n(-\infty) = 1 - 0 = 1, \quad (25)$$

$\mathbb{E}(M'_n)$ is a re-weighting of different x -s and the weight for $\max(\Delta)$ is not 1, hence $\mathbb{E}(M'_n) < \max(\Delta)$. However, as $n \rightarrow \infty$, $(F^n(x) - F^n(x^-)) \rightarrow 0$ for all $x \neq \max(\Delta)$, so

$$\mathbb{E}(M'_n) \xrightarrow{d} \max(\Delta) \text{ as } n \rightarrow \infty, \quad (26)$$

making $\{M'_n\}_{i=1}^\infty$ asymptotically unbiased. Recall notations from Section 2, given n realizations $\{\delta_i\}_{i=1}^n$ of the random variables $\{\Delta_i\}_{i=1}^n$,

$$\mu_\delta = \frac{\sum_{i=1}^n \delta_i}{n} \quad (27)$$

and

$$\delta_{\min} = \min(\{\delta_i : i = 1, \dots, n\}) \quad (28)$$

are our final estimation of the mean and minimum of Δ . Our weak and strong law are designed to fit those estimations. To be specific, each fitting of the weak or the strong law tries to fit separately on μ_δ and δ_{\min} , which is also why each of our laws has two separate parts for expectation and minimum values.

H ADDITIONAL RELATED WORK

In addition to the backgrounds presented in Section 4, we further discuss the related work on mixed precision. Specifically, we categorize the work under the following three topics: mixed-precision quantization, mixed-precision inference, and mixed-precision training.

Mixed-precision quantization Mixed precision approaches involve partitioning a model’s parameters into both high-precision and low-precision components, which have been shown to better preserve model performance relative to uniform quantization. This is primarily seen in models that exhibit different sensitivities to quantization at various layers. Some mixed-precision LLM quantization work adopts the concept of weight salience to guide the search for fine-grained bit allocation. The first-order (Li et al., 2023) or second-order weight gradient (Huang et al., 2024) has been used to form such salience metrics, such that salient layers are left in higher precision while the rest are cast to low precision. There are also works performing the search in an end-to-end style with the quantized model performance as the objective, such as the accuracy on a downstream task (Zhang et al., 2023a). In both cases, mixed precision can be seen as a promising approach to provide a loss-less reduction in LLM memory requirements, reducing average bit widths below levels achievable through uniform quantization.

Mixed-precision inference Mixed-precision inference methods targeting GPUs usually adopt regular mixed-precision strategies and computation patterns; The authors of GPTQ3.int8() (Dettmers et al., 2022) decompose the matrix multiplication in every linear layer into two sub-matrix-multiplications based on the activation magnitudes, achieving a 2-3 \times inference speedup by casting the low-magnitude sub-matrix to low precision. SpQR (Dettmers et al., 2023) represents a weight matrix with grouped 3-bit integers and less than 1% sensitive weight elements with FP16 values, achieving a 2 \times speedup compared to a quantized and sparse PyTorch baseline. These approaches enable reducing model size, but additional careful treatment is needed to improve inference throughput. For example, in (Li et al., 2023), mixed precision LLM quantization at 2-bit and 3-bit showed no speedup compared to 4-bit, due to less efficient utilization of memory bandwidth. On the other hand, Any-Precision LLM (Park et al., 2024) achieves throughput scaling at various precisions by providing CUDA kernels with a novel weight packing approach following a bitplane layout, achieving 1.3-1.8 \times speedup on mobile and edge devices. Additionally, works such as FlightLLM achieve high throughput by leveraging custom hardware designs (Zeng et al., 2024).

Mixed-precision training Mixed-precision quantization has also been adopted in training to reduce the large memory footprint of gradient descent, which requires the storage of optimizer states and gradients in addition to forward activations. It has been shown that the training process can

tolerate aggressive quantization and correct quantization noise in some components. (Micikevicius et al., 2017) is the pioneering work proposing the storage of all weights, activations, and gradients in FP16, while updating a copy of weights in FP32. This work also proposed scaling up the forward pass loss and unscaling the gradient before the weight update to avoid under-utilization of the FP16 representable range, leading to half the memory requirement and speed-ups of $2\text{-}6\times$ relative to FP32 training. Recently, more aggressive quantization has been studied for mixed-precision training. (Mellempudi et al., 2019) trains models with E5M2 FP8, maintaining a master copy of the weights in FP16, and dynamically adjusting the scaling factor every few iterations. Hybrid-FP8 (Sun et al., 2019) improves FP8 training by using E4M3 for forward propagation and E5M2 for backward propagation, leading to matching performance to models trained with FP32. Popular implementations of FP8 mixed-precision training like TransformerEngine² have achieved a training acceleration of around $3\text{-}4\times$ compared to FP16 mixed-precision training.

²TransformerEngine: <https://github.com/NVIDIA/TransformerEngine>.